이학박사 학위논문

Single-Molecule FRET Studies on Z-DNA

단일분자 프렛을 이용한 Z-DNA 연구

2012 년 8 월

서울대학교 대학원

물리천문학부

배 상 수

Single-Molecule FRET Studies on Z-DNA

지도 교수 홍 성 철

이 논문을 이학박사 학위논문으로 제출함
2012 년 6 월

서울대학교 대학원
물리천문학부
배 상 수

배상수의 이학박사 학위논문을 인준함
2012 년 6 월

위 원 장 박 건 식 (인)

부위원장 홍 성 철 (인)

위 원 홍 승 훈 (인)

위 원 김 대 식 (인)

위 원 김 양 균 (인)

Ph.D. Dissertation

Single-Molecule FRET Studies on Z-DNA

Sangsu Bae

***Research Advisor*: Professor Sungchul Hohng**

August 2012

School of Physics and Astronomy

Seoul National University

Abstract

Single-Molecule FRET Studies on Z-DNA

Sangsu Bae
Major in Biophysics
Department of Physics and Astronomy
The Graduate School
Seoul National University

It has been advanced to study biology in a molecular level for the last century. Especially, a new field 'Molecular Biology' appeared after Watson and Crick proposed the DNA's helical structure in 1953. DNA structure which Watson and Crick proposed was called B-formed DNA and it was built up the right-handed double helical structure. This structure had been confirmed by many different studies and became realistic.

However, in 1979, not right handed DNA but left handed DNA (Z-DNA, named by zigzag backbone structure) was observed in the first atomic resolution view of the double helix by A. Rich group. Unlike B-DNA, Z-DNA had many different things. The helical structure of Z-DNA was left-handed and Z-DNA was thinner and more extended than B-DNA. While Z-DNA is formed with a very brief lifetime under normal conditions, it has been known

that various factors such as high salt concentration, negative supercoiling, chemical modifications of bases, and Z-DNA binding proteins can make the threshold salt concentration for B-to-Z transition goes down to physiological levels. From enormous experimental data accumulated over the past 30 years, Z-DNA is thought to play fundamental roles such as regulatory at the transcriptional step, nucleosome positioning, and genetic instability.

In previous ensemble studies, a little portion of Z-DNA surrounded with B-DNA at each side was limited to measure due to large signal of B-DNA. Therefore, studies of Z-DNA with BZ junction was rare. To overcome this problem, we employed single-molecule FRET assay and was successful to distinguish B-DNA and Z-DNA. From this assay, we were able to observe B-to-Z transition with high salt and Z-DNA binding protein. In this paper,

i) We examined the Z-DNA stabilizing capabilities of different salts by using single-molecule experiments along with circular dichroism measurements. Contrasted to the prediction of the widely accepted model of electrostatic screening, strong correlation between the degree of helix-to-coil transition and B-to-Z transition revealed that B-to-Z transition follows the Hofmeister series. And we also measured energetics of salt-induced Z-DNA formation. As a result, surprisingly, the effect of BZ junction was so dramatic that thermodynamic properties were inverted in whole when BZ junction was added, e.g. enthalpic term helped B-DNA to transform to Z-DNA and entropic term hindered the B-to-Z transition if there was no BZ junction, but entropic term helped B-to-Z transition with BZ junction.

ii) We were able to observe intrinsic B-Z transitions, protein association/dissociation events. These results revealed that intrinsic B-Z transitions were dynamically formed and Z-DNA was effectively stabilized by Z-DNA binding proteins through passive role of protein, rather than active role of it. Our study provided, for the first time, detailed pictures of the intrinsic B-Z transition dynamics and protein-induced B-to-Z transition mechanism at the single molecule level.

iii) We successfully measured equilibrium constant of double-stranded (ds) DNA, dsRNA, DNA-RNA hybrid sample at various temperature. From fitting with van't Hoff equation, we calculated enthalpic and entropic change of B-Z transition as well as free energy. From these results, we proposed linear model system and calculated energy of (CG) and junction at each. As a result, hybrid sample was fastest and easiest to transform to Z-form due to lower junction free energy barrier. It meant that substrate of so-called Z-DNA binding protein might be RNA or hybrid as well as DNA.

Keywords: Z-DNA, BZ transition, Z-DNA binding protein, Single-molecule fluorescence resonance energy transfer (FRET), Hofmeister effect, DNA-RNA hybrid

Student Number: 2008-30118

Contents

Abstract

Contents

Chapter 1. Introduction..……..…….1

1.1. Single-Molecule FRET……..…….1

1.1.1. Fluorescence Resonance Energy Transfer……..…….....…1

1.1.2. Single-molecule FRET assay…….……2

1.2. Z-DNA……4

1.2.1. Discovery of Z-DNA……..…….....…4

1.2.2. High salt condition…….……5

1.2.3. Negative supercoiling…….……..…….....…5

1.2.4. Z-DNA binding protein…….…….……6

1.3. References…….……7

Chapter 2. B-to-Z transition mechanism under high salt concentration

…….……10

2.1. Introduction…….……10

2.2. Materials and Methods……..…12

2.2.1. Sample preparation…….…….....12

2.2.2. Experimental methods……13

2.3. Results……..……17

2.3.1. Z-DNA quantification via smFRET..…....……..…17

2.3.2. Comparison of Z-DNA inducing capabilities of various salts

…….…… 24

2.3.3. Generality of Hofmeister series in B-to-Z transition ……27

2.4. Discussions……33

2.5. References……40

Chapter 3. Energetic information of Z-DNA at high salt concentration ……..37

3.1. Introduction……..37

3.2. Results……39

3.2.1. BZ transition of various DNA samples.....….....39

3.2.2. Energetics for junction, (CG) repeats…….....44

3.3. Discussions.....50

3.4. References……...51

Chapter 4. B-to-Z transition mechanism via Zα protein……...52

4.1. Introduction……...52

4.2. Materials and Methods……53

4.2.1. sample preparation……53

4.2.2. Experimental methods……54

4.3. Results and Discussions……..……55

4.3.1. Stepwise B-to-Z transitions occur with time delays after Zα binding ……..……..……55

4.3.2. B-to-Z transition rates in the presence of ZBPs are identical to the intrinsic B-to-Z transition rates ……..……..……62

4.3.3. Z-DNAs are stabilized by selective trapping of transient Z-DNAs by ZBPs ……..……..……..……...70

4.4. References ……...……75

Chapter 5. Energetics of different duplexes- DNA, RNA, and hybrid.....78

5.1. Introduction……..78

5.2. Materials and Methods…….…...……80

5.2.1. Protein, DNA, RNA, and Hybrid sample preparation…….……80

5.2.2. Experimental methods.…….…...…80

5.2.3. Analysis -Determination of thermodynamic parameters….……81

5.3. Results…….…….39

5.2.1. Z-form of DNA-RNA hybrid is most efficiently stabilized by ZBP……82

5.2.2. Z-form is favoured at higher temperatures.…….……88

5.2.3. DNA-RNA hybrid has the lowest junction energy…….…….98

5.4. Discussions…….101

5.5. References……..102

Abstract in Korean (국문초록).…….…….106

Chapter 1. Intruction

1.1. Single-Molecule FRET

1.1.1. Fluorescence Resonance Energy Transfer

FRET is the non-radiative energy transfer from excited states of one fluorophore (donor) to another (acceptor). This means that the energy transfer occurs without the appearance of a photon. The essence of this energy transfer is a dipole-dipole interaction between donor and acceptor. Therefore the spectral overlap between donor emission and acceptor absorption is basically required. Mechanism of the energy transfer was first calculated by T. Förster [1] and the FRET efficiency E is expressed by [2]

$$E = \frac{1}{1 + (R_0/R)^6}$$

, where distance R_0 called Förster distance at which half of energy was transferred. And after correcting the value by the quantum mechanical consideration, R_0 can be written as

$$R_0{}^6 = (8.785 \times 10^{-25})\Phi_D \kappa^2 n^{-4} J(\nu) cm^6$$

, where Φ_D is the quantum yield of donor dye, κ is the orientation factor of dipole-dipole interaction, $J(\nu)$ is the integral of the spectral overlap, n is the refractive index of the medium.

On the other hand, in single molecule dual channel detection, FRET efficiency can be calculated by [3]

$$E = \frac{I_A}{I_D + \frac{\Phi_A \eta_A}{\Phi_D \eta_D} \times I_A}$$

, where I_A is the acceptor intensity, I_D is the corresponding donor intensity, Φ_D and Φ_A is denoted the fluorescence quantum yields for donor and acceptor, and η_D and η_A is collection efficiencies for donor and acceptor channels, respectively.

1.1.2. Single-molecule FRET assay

Single-molecule FRET detection has many advantages compared with ensemble (or bulk) FRET measurement. In single-molecule FRET assay, it is possible to detect molecular heterogeneity, whereas only averaged results are showed in ensemble FRET assay. Moreover, due to the detection of each single-molecule, study of molecular dynamics is possible.

In single-molecule FRET assay, there are several types as to the type of incident laser, epi, HILO, and TIRF (total internal reflection fluorescence) miocroscopy. Among them, TIRF microscopy has benefits that the background signal in aqueous solution are reduced and magnitude of incident laser is increased. And in TIRF microscopy, there are two different types. One is prism-type TIRF microscopy and the other is objective-type TIRFM or prismless TIRFM [4].

In single-molecule FRET assay, a quartz slide is coated with poly-ethylene glycol (PEG) and streptavidin. After immobilizing biotinylated DNA on the surface, images are obtained in a wide-field total-internal-reflection fluorescence microscope with 100-ms time resolution using an electron

multiplying charge-coupled device (EM-CCD) camera as shown in Fig. 1.1 [5].

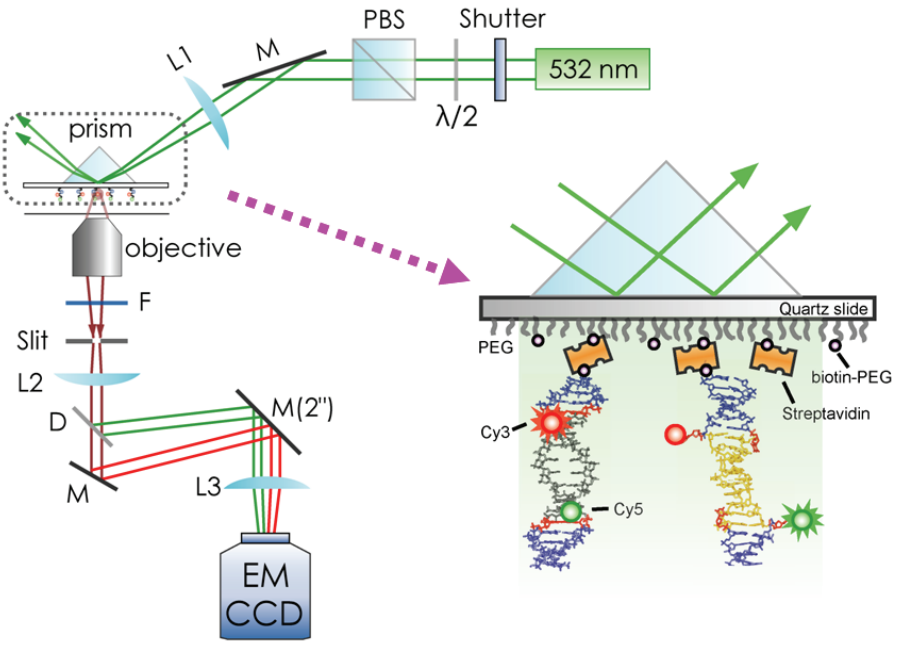

Figure 1.1. Schematics of Prism-type TRIF micorscpe

1.2. Z-DNA

Watson and Crick first proposed DNA model that had the structure of right-handed double helix (called B-DNA) in 1953 [6]. But it was not until the 1970's, that another DNA structure was found. In 1972 Pohl and Jovin found that the ultraviolet Circular Dichroism spectrum of poly(dG-dC) nearly inverted to established B-DNA in 4M NaCl [7].

1.2.1. Discovery of Z-DNA

In 1979, when DNA synthesis was developed, first single-crystal x-ray diffraction of DNA was revealed DNA structure not to B-formed DNA but to left handed DNA (called Z-DNA, named by zigzag backbone structure) interestingly [8]. Unlike B-DNA, the structure of Z-DNA had many different things. The helical structure of Z-DNA was left-handed and the phosphate groups pursued a zig-zag course along the backbone. And the sugar residues had an alternating orientation and the minor groove of Z-DNA was below the base pairs, whereas in B-DNA, the minor groove was above the base pairs. And Z-DNA was also thinner and more extended than B-DNA.

After discovery of Z-DNA, the biological meaning of Z-DNA as well as many factors of stabilizing Z-DNA have been reported. It is known that Z-DNA is well stabilized by the help of high salt condition, negative supercoiling, and Zα-protein.

1.2.2. High salt condition

After the first recognition of Z-DNA, detected by ultraviolet Circular Dichroism spectrum in 4M NaCl condition, several studies confirmed the results that Z-DNA was well stabilized in such a high salt condition, not only NaCl but other cations or anions) [9, 10]. And it was also confirmed that Z-DNA detected in high salt condition had a same construct of crystal structure revealed in 1979 by A. Rich group [11].

In high salt condition, it has been widely thought that Z-DNA is stabilized in high salt conditions due to the conformation of Z-DNA [12]. The conversion of B-DNA to Z-DNA was associated with a 'flipping over' of the base pairs so that base pair of Z-DNA had up upside down orientation relative to that of B-DNA. The net result of this reorganization caused that phosphate groups were closer together in Z-DNA than in B-DNA. Therefore, under standard cellular conditions, the electrostatic repulsion of these charged phosphate groups would push the molecule into the B-DNA conformation. But in the presence of high-salt solution, the electrostatic repulsion of the phosphate residues was vastly decreasing so that Z-DNA became the stable conformation. However, recent data demonstrated the reason of salt-induced Z-DNA to Hofmeister effect, not electrostatic effect of high salts in water.

1.2.3. Negative supercoiling

It was found that negative supercoiling as well as high salt made it easier to stabilize Z-DNA [13,14]. This finding indicated the biological roles at

transcription or chromatin remodeling processes because negative supercoiling is typically observed in the cellular condition during at transcription or chromatin remodeling processes [15,16].

The fact that negative supercoiling stabilizes Z-DNA may be a key to understand many unknown problems in a cell. Because DNA is wrapped and packaged with a protein, Histone as negatively supercoiled and some stress applied to DNA during transcription or recombination can be decreased by inducing Z-DNA. And the fact that the ~80% of sequences which can be converted to Z-DNA exist at the sites of promoter region in human chromosome may imply the biological role of Z-DNA at transcription or chromatin remodeling processes [17].

In 1986, Lawrence J. Peck *et al.* calculated the rate of B to Z structural transition [18]. As a result, more negatively supercoiled DNA sample can be converted to Z-DNA more quickly. On the other hand, below superhelical density σ=-0.05, the transition of B to Z occurs slowly.

1.2.4. Z-DNA binding protein

In 1990's, some proteins which was able to bind to Z-DNA with high specificity were discovered. Thomas Schwartz *et al*. reported by the crystal structure that editing enzyme double-stranded RNA adenosine deaminase (ADAR1) included a DNA binding domain, Zα, which was specific to the left-handed Z-DNA [19]. It was also found that DAI (or DLM1), E3L, and PKZ as well as hZα_{ADAR1} had a similar sequence motifs, Zα [20-23]. Like

other pathogen associated molecular pattern (PAMP), the formation of Z-DNA in cytosol seemed to evoke expression of type I IFN through its cytosolic receptor, DAI. Recently, the novel function of ADAR1 as immune suppressor was reported. Knock down of ADAR1 showed increased expression of IFN under viral infected condition [24]. And E3L which was discovered in poxviruses and vaccinia virus was necessary for pathogenicity.

1.3. References

[1] T. Förster, *Annalen der Physik* **1948**, 437, 55-75.

[2] S. Weiss, *Science* **1999**, 283, 1676-1683.

[3] T. Ha, *Methods* **2001**, 25, 78-86.

[4] C. Joo, H. Balci, Y. Ishitsuka, C. Buranachai, T. Ha, *Ann. Rev. Biochem.* **2008**, 77, 51-76.

[5] R. Roy, S. Hohng, T. Ha, *Nat. Methods* **2008**, 5, 507-516.

[6] J. D. Watson, F. H. C. Crick, *Nature* **1953**, 171, 737-738.

[7] F. M. Pohl, J. M. Jovin, *J. Mol. Biol.* **1972**, 67, 375-396.

[8] A. H.-J. Wang, G. J. Quigley, F. J. Kolpak, J. L. Crawford, J. H. van Boom, G. van der Marel, A. Rich, *Nature* **1979**, 282, 680-686.

[9] M. Behe, S. Zimmerman, G. Felsenfeld, *Nature* **1981**, 293, 233-235.

[10] A. Rich, A. Nordheim, A. H. Wang, *Ann. Rev. Biochem.* **1984**, 53, 791-846

[11] T. J. Thamann, R. C. Lord, A. H. -J. Wang, A. Rick, *Nucl. Acids Res.* **1981**, 9, 5443-5457.

[12] A. Rich, S. Zhang, *Nat. Rev. Genet.* **2003**, 4, 566-572.

[13] L. J. Peck, A. Nordheim, A. Rich, J. C. Wang, *Proc. Natl. Acad. Sci. USA* **1982**, 79, 4560-4564.

[14] A. R. Rahmouni, R. D. Wells, *Science* **1989**, 246, 358-363.

[15] B. Wittig, S. Wölfl, T. Dorbic, W. Vahrson, A. Rich, *EMBO J.* **1992**, 11, 4653-4663.

[16] R. Liu, H. Liu, X. Chen, M. Kirby, P. O. Brown, K. Zhao, *Cell* **2001**, 106, 309-318.

[17] G. P. Schroth, P. J. Chou, P. S. Ho, *J. Biol. Chem.* **1992**, 267, 11846-11855

[18] L. J. Peck, J. C. Wang, A. Nordheim, A. Rich, *J. Mol. Biol.* **1986**, 190, 125-127.

[19] T. Schwartz, M. A. Rould, K. Lowenhaupt, A. Herbert, A. Rich, *Science* **1999**, 284, 1841-1845.

[20] A. Herbert, K. Lowenhaupt, J. Spitzner, A. Rich, *Proc. Natl. Acad. Sci. USA* **1995**, 92, 7550-7554.

[21] T. Schwartz, J. Behlke, K. Lowenhaupt, U. Heinemann, A. Rich, *Nat. Struct. Biol.* **2001**, 8, 761-765.

[22] S. Rothenburg, N. Deigendesch, K. Dittmar, F. Koch-Nolte, F. Haag, K. Lowenhaupt, A. Rich, *Proc. Natl. Acad. Sci. USA* **2005**, 102, 1602-1607.

[23] Y. -G. Kim, M. Muralinath, T. Brandt, M. Pearcy, K. Hauns, K.

Lowenhaupt, B. L. Jacobs, A. Rich, *Proc. Natl. Acad. Sci. USA* **2003**, 100, 6974-6979.

[24] A. Takaoka, Z. Wang, M. K. Choi, H. Yanai, H. Negishi, T. Ban, Y. Lu, M. Miyagishi, T. Kodama, K. Honda, Y. Ohba, T. Taniguchi, *Nature* **2007**, 448, 501-505.

[25] S. C. Ha, N. K. Lokanath, D. Van Quyen, C. A. Wu, K. Lowenhaupt, A. Rich, Y. -G. Kim, K. K. Kim, *Proc. Natl. Acad. Sci. USA* **2004**, 101, 14367-14372.

Chapter 2. B-to-Z transition mechanism under high salt concentration

2.1. Intruction

Specificity is a premise of life and highly specific interactions are ubiquitous DNA is a highly polymorphic molecule, whose conformational transitions are intimately related to the regulation of various biological processes [1-3]. Understanding of physical driving forces responsible for these DNA structural changes is an important unsolved issue of molecular biophysics. Z-DNA, a left-handed isoform of Watson-Crick's B-DNA, is formed in purine-pyrimidine repeats at high salt conditions [4,5]. While Z-DNA is formed with a very brief lifetime under normal conditions, it is well known that various factors such as negative supercoiling, chemical modifications of bases, and Z-DNA binding proteins—all of them are physiologically relevant—can make the threshold salt concentration for B-to-Z transition goes down to physiological levels [6,7]. From enormous experimental data accumulated over the past 30 years, Z-DNA is thought to play fundamental roles such as regulatory at the transcriptional step and nucleosome positioning [8-12].

Compared to these progresses in structural and biological studies of Z-DNA, a physical understanding of how Z-DNA is stabilized by various physical factors is still lacking [13]. It is widely accepted that Z-DNA is stabilized by salts via the electrostatic screening mechanism based on the

following observations. First, the crystallization of Z-DNA revealed that the phosphate groups were positioned closer in Z-form than in B-form. Therefore, the electrostatic repulsion between negatively charged phosphate groups seems to be more severe in Z-form than in B-form DNA, and more concentrated cations are required to reduce it [4.7]. Second, multivalent cations were generally more efficient in inducing Z-DNA than monovalent ones [5,14]. Although some observations that did not fit into this simple screening model were reported, they were considered as exceptional, and the screening mechanism itself has never been seriously questioned yet [5,14-16].

In this work, we quantitated Z-DNA population at various salt conditions by using single-molecule fluorescence resonance energy transfer (FRET) technique [17] along with bulk FRET and circular dichroism (CD) measurement. And surprisingly we observed that B-to-Z transition followed Hofmeister effect rather than electrostatic (coulombic) effect.

Salt in solution with bio-molecule can have different roles, electrostatic effect, or Hofmeister effect. Since Franz Hofmeister discovered the participation effect of various salts for egg protein [18], so-called Hofmeister series of salt effects have been observed in broad range of fields, e.g. enzyme activity, protein stability, surface tension, micelle formation, bacterial growth, or DNA denaturing, so on [19-21]. Despite the generality of these specific effects, understanding on molecular level is still limited. Here, we report that B-to-Z transition induced by salt is an another example of Hofmeister effect and offer the clue on B-to-Z transition mechanism on molecule-level.

2.2. Materials and Methods

2.2.1. Sample preparation

For the single molecule FRET experiment, modified oligonucleotides were purchased from Integrated DNA Technologies (Coralville,IA). We prepared a DNA duplex, named $B(CG)_6B$, with six CG-repeats in the middle (underlined in the sequence below), and 10 base pairs flanking random-sequence regions, by annealing the following two strands:

5'-/biotin/-CCCAGTTGATCy5CGCGCGCGCGCGATAACCCACC-3', and 5'-GGTGGGTTATCy3CGCGCGCGCGCGATCAACTGGG-3'. The anime-modified thymine bases (bald character) at BZ junction, which are flipped out in Z-DNA, were selected as a labeling position of fluorophores so that maximum FRET change occurs when the CG repeat switches into Z-DNA. DNA duplex were annealed by mixing the biotinylated and non-biotinylated stand in 1:2 ratio at 50 μM concentration in a buffer containing 10mM Tris (pH 8.0) and 50mM NaCl. The non-biotinylated strand was added in excess to minimize the chance of having un-annealed biotinylated strand in single-molecule measurement. The annealing mixture was heated at 95 ºC for 3 minutes and allowed to cool down slowly for 1.5 hours in a heating block. And control sample was prepared with same formula but no CG-repeats, named B_{con}, by annealing the following two strands:

5'-/biotin/-CCCAGTTGATCy5TATGCAATCGTAATAACCCACC-3', and 5'-GGTGGGTTATCy3TACGATTGCATAATCAACTGGG-3'. DNA duplex were annealed by the same method with $B(CG)_6B$.

For the circular dichroism (CD) experiment, non-modified oligonucleotides were purchased from Bioneer (Korea). We prepared a DNA duplex, with six CG-repeats in the middle and five base pairs flanking random-sequence regions for increasing the Z-DNA detection efficiency, by annealing the following two strands:

5'-GTCATCGCGCGCGCGATAAC-3', and

5'-GTTATCGCGCGCGCGATGAC-3'. DNA duplex were annealed by mixing the stand in 1:1 ratio at 500 μM concentration in a buffer containing 10mM Tris (pH 8.0) and 50mM NaCl.

For bulk FRET experiment on DNA denaturing, we prepared a 12-bp DNA duplex, named B_{12bp}, by annealing the following two strands, respectively:

5'-/Cy5/ TATGCAATCGTAATAAACCGT-/biotin/-3', and

5'-/Cy3/ TACGATTGCATA-3'. Cy3 and Cy5 dyes were labeled at the same ends of the duplex and DNA duplex were annealed by mixing the Cy5-labeled and Cy3-labeled stand in 1.5:1 ratio at 50 μM concentration in a buffer containing 10mM Tris (pH 8.0) and 50mM NaCl. The Cy5-labeled strand was added in excess to minimize the chance of having free Cy3-labeled single strand in measurement.

2.2.2. Experimental methods

A sample chamber with narrow width <1cm was made by assembling the quarts slide and glass cover-slip using double-sided adhesive tape and epoxy.

Biotinylated DNA molecules (80pM) were immobilized on a quartz slide coated with poly-ethylene glycol (PEG) and streptavidin. Then images were obtained in a wide-field total-internal-reflection fluorescence microscope with 100-ms time resolution using an electron multiplying charge-coupled device (EM-CCD) camera (iXon DV887ECS-BV, Andor Technology) and a homemade C++ program. Measurements were performed at 25 ºC. As an oxygen scavenger system to slow photobleaching, we injected the imaging buffer included 10mM Tris-HCl (pH 8.0, 1% (v/v) Trolox (Sigma-Aldrich), 0.4% D-glucose (Sigma-Aldrich), 1 mg/ml glucose oxidase (Sigma-Aldrich) and 0.04 mg/ml catalase (Roche, Nutley, NJ) with designated ions. All single-molecule experiments were done at RT (24~25 ºC).

Fluorescence spectroscopy

Bulk FRET efficiency were determined using Varian Eclipse fluorescence spectrophotometer. Same sample prepared for smFRET was used in this experiment. DNA duplex (10nM) was incubated in buffer containing 10mM Tris-HCl (pH 8.0) with designated ions at 25 ºC. Cy3 was excited by light with 532nm wavelength. Emission wavelength peak for Cy3 and Cy5 were set as 565nm and 665nm, respectively. FRET efficiency was calculated by $I_{665nm}/(I_{565nm}+I_{665nm})$. I_{peak} means the fluorescence intensity of the peak. All bulk experiments were done at 28 ºC.

Circular Dichroism

CD spectra were recorded using by a Jasco-815 spectropolarimeter through using a quarts cell with an optical path length of 1 mm in the wavelength range of 240~310 nm at 25 ºC; the band width 1 nm, the scanning speed 50 nm/min and the response time 8s. DNA duplex were diluted into 5 μM by 10 mM Tris (pH 8.0) and 50 mM NaCl. All CD experiments were performed at 25 ºC.

Table 2.1. Various DNA samples

DNA name	sequences
$B(CG)_6B$	5'-/biotin/-CCCAGTTGAT**T**^{Cy5}CGCGCGCGCGCGATAACCCACC-3' 5'-GGTGGGTTAT**T**^{Cy3}CGCGCGCGCGCGATCAACTGGG-3'
$B(CG)_6$	5'-/Cy5/ CGCGCGCGCGCGATAACCCACC /biotin/-3' 5'-GGTGGGTTAT**T**^{Cy3}CGCGCGCGCGCG-3'
$(CG)_6$	5'-/Cy5/ CGCGCGCGCGCGATAACCCACC /biotin/-3' 5'-/Cy3/ CGCGCGCGCGCG -3'
$B(CG)_6B\_con$	5'-/biotin/-CCCAGTTGAT**T**^{Cy5}TATGCAATCGTAATAACCCACC-3' 5'-GGTGGGTTAT**T**^{Cy3}TACGATTGCATAATCAACTGGG-3'
$B\ (CG)_6\_con$	5'-/Cy5/ TATGCAATCGTAATAAACCGT /biotin/-3' 5'-ACGGTTTAT**T**^{Cy3}TACGATTGCATA-3'
B_{12bp}	5'-/Cy5/ TATGCAATCGTAATAAACCGT-/biotin/-3' 5'-/Cy3/ TACGATTGCATA-3'
$B(CG)_6B\_CD$	5'-GTCATCGCGCGCGCGCGATAAC-3'

	5’-GTTATCGCGCGCGCGCGATGAC-3’
$B(CG)_6$_CD	5’- CGCGCGCGCGCGATAACCCACC-3’ 5’-GGTGGGTTATCGCGCGCGCGCG-3’
$(CG)_6$_CD	5’- CGCGCGCGCGCG-3’ 5’- CGCGCGCGCGCG-3’
B_{con}_CD	5’- TATGCAATCGTAATAAACCGT -3’ 5’-ACGGTTTATTACGATTGCATA-3’

2.3. Results

2.3.1. Z-DNA quantification via smFRET

To characterize BZ transition at different salt conditions, we carried out single-molecule FRET experiment. For these measurements, we prepared a DNA duplex, named $B(CG)_6B$, with six CG-repeat in the middle [gray and yellow in Fig. 2.1(b)], and flanking random-sequence regions [blue in Fig. 2.1(b)] as shown in Fig. 2.1(a). The thymine bases at BZ junction were selected as a labeling position of fluorophores for maximum FRET change during B-Z transition [22,23].

Annealed DNA molecules were immobilized on a polymer-coated quartz surface by biotin-streptavidin interaction, and fluorescence signals of donor and acceptor were obtained in a wide-field total-internal-reflection fluorescence microscope (TIRFM) [24]. As shown in Fig. 2.1(c), FRET histograms at different $NaClO_4$ concentrations were obtained. Below 3M $NaClO_4$, FRET histograms were dominated by a single Gaussian distribution, confirming the existence of a single conformation, i.e. B-DNA. Above 3M $NaClO_4$, however, a new FRET state started to appear at around 0.4, and became a dominant portion at higher salt concentrations. In control experiments with a DNA duplex which cannot form Z-DNA, the low FRET state didn't emerge (Fig. 2.2) confirming the identity of the low FRET state as Z-DNA. CD measurements indicated that B-to-Z transition occurs at similar $NaClO_4$ concentrations (Fig. 2.3), also confirming that single-molecule FRET

can reliably report BZ transition.

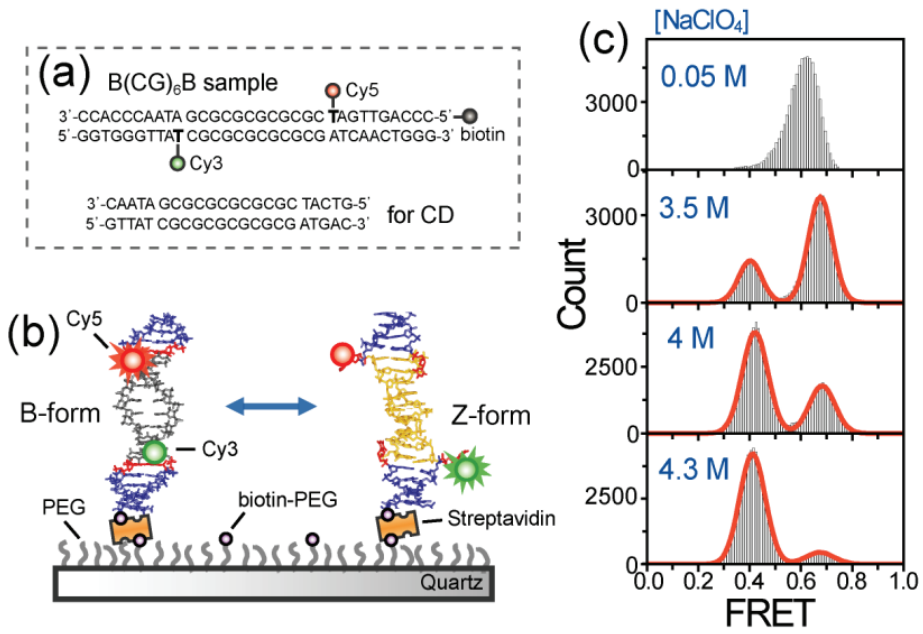

Figure 2.1. Single molecule FRET assay. (a) DNA sequences, named $B(CG)_6B$, for single-molecule FRET and circular dichroism (CD) studies. In CD experiment, non-modified oligonucleotides flanking short random-sequence regions was used for increasing the Z-DNA detection efficiency. (b) A schematic diagram of single-molecule FRET experiments. (c) FRET histograms of $B(CG)_6B$ sample at various $NaClO_4$ concentrations.

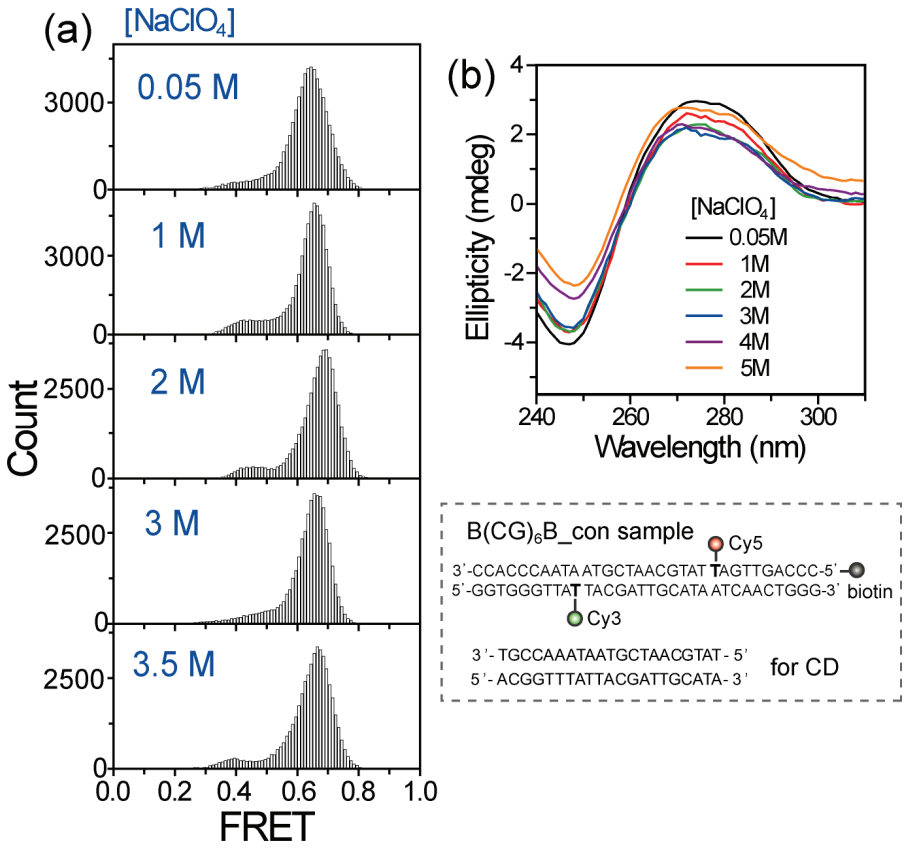

Figure 2.2. Control experiments on a random DNA duplex. (a) FRET histograms of $B(CG)_6B$_con sample at various $NaClO_4$ concentrations. No FRET change assigned to Z-DNA was observed in this sample. (b) CD spectra of the random duplex at various $NaClO_4$ concentrations. For CD measurement, non-modified DNA sample was prepared and DNA sequences of the duplex are shown at the bottom. Consistently with single-molecule FRET measurements, no structural transition was observed.

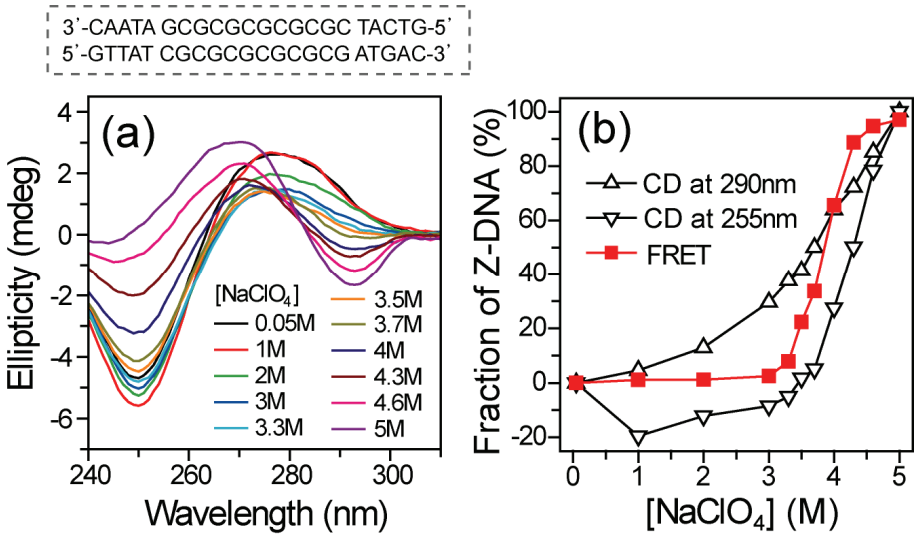

Figure 2.3. CD data with B(CG)6B_CD sample. (a) CD spectra of $B(CG)_6B$_CD sample at various $NaClO_4$ concentrations. DNA sample for CD measurement was shown at top of the figure. In CD experiment, non-modified oligonucleotides flanking short random-sequence regions was used for increasing the Z-DNA detection efficiency. (b) Fraction of Z-DNA was calculated from single-molecule measurements [red squares, Fig 2.1(c)], and CD measurements at 255-nm (lower triangles), and at 290-nm (upper triangles) from (a). Fraction of Z-DNA calculated from CD measurements at 255-nm and at 290-nm was not same each other, i.e. the CD signal is not a simple linear sum of B-form and Z-form. In conclusion, single-molecule FRET approach is more accurate in Z-DNA quantity.

To compare Z-DNA-inducing capabilities of different salts, we repeated the titration experiments with various salts. As shown in Fig. 2.4(a), contrary to the prediction of the screening model, it was of interest that Z-DNA was not observed at all by $MgCl_2$ even at saturating concentrations. Because, by the screening model, an anion's effects was expected to be negligible with a negatively charged DNA, it was limited to explain with this model.

Alternatively, we assumed that an anion (ClO_4^-) plays a determining role in Z-DNA stabilization. Indeed, when an anion of $MgCl_2$ (Cl^-) was replaced with (ClO_4^-), Z-DNA was induced at much lower concentrations [Fig. 2.4(b)]. Another surprising observation from a viewpoint of screening is that $Ca(ClO_4)_2$, a less effective salt in electrostatic screening than $Mg(ClO_4)_2$, was more efficient than $Mg(ClO_4)_2$ in inducing Z-DNA [Fig. 2.4(b)-(c)], indicating a direct contradiction to the simple screening model. CD spectra also showed similar consequences (Fig. 2.5). Fig. 2.4(d) summarized the fraction of Z-DNA with various salt concentrations and all the findings in Fig. 2.4(d) cannot be compatible with the screening model. Rather they seem to be consistent with the Hofmeister effect. Indeed, it is well known that anions play an dominant role in the Hofmeister effect.

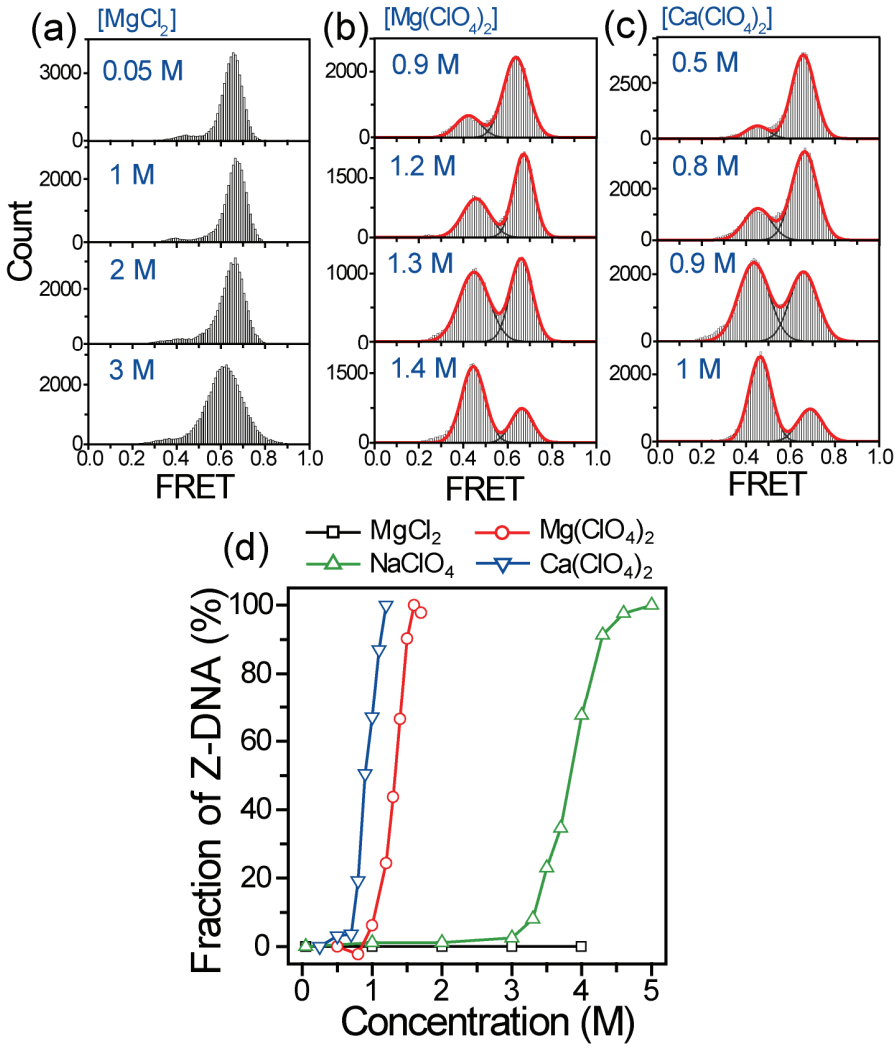

Figure 2.4. BZ transition induced by various salts. (a), (b), and (c) FRET histograms of $B(CG)_6B$ at designated concentrations of various salts. (d) Z-DNA-inducing capabilities of different salts. Fraction of Z-DNA were obtained by FRET histogram and plotted as a function of salt concentration.

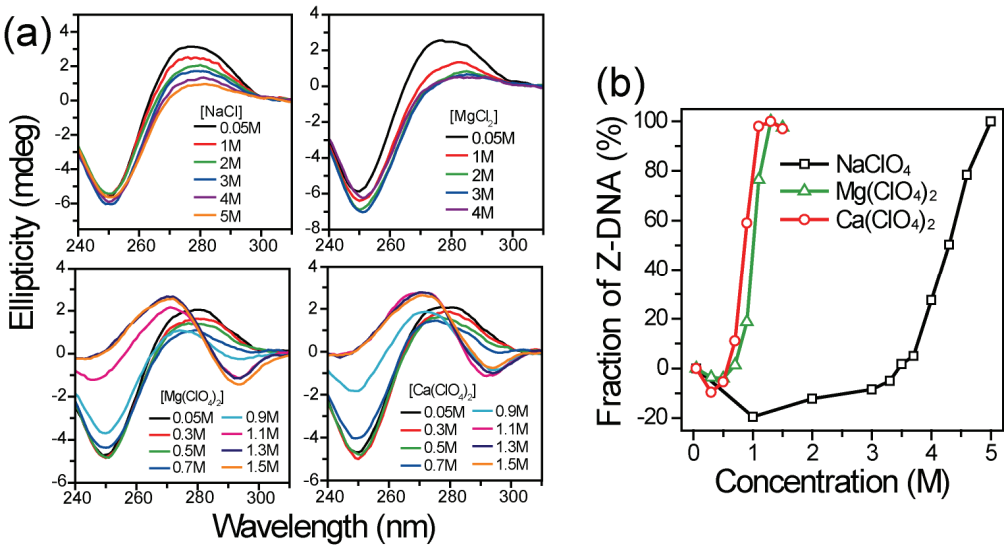

Figure 2.5. CD spectra at various salt condition. (a) CD spectra of $B(CG)_6B$ at various NaCl, $MgCl_2$, and $Mg(ClO_4)_2$, and $Ca(ClO_4)_2$ concentrations, respectively. DNA duplex was prepared to have five base pairs flanking random-sequence regions for increasing the Z-DNA detection efficiency, named $B(CG)_6B$_CD. DNA sequences of the duplex are shown at Table 2.1. As a result, it is of interest that $MgCl_2$ cannot induce BZ transition at all. (b) Summarized BZ transition graph. The tendency is as same as the result from single-molecule FRET histogram [Fig. 2.4(d)].

2.3.2. Comparison of Z-DNA inducing capabilities of various salts

To test whether the salt-induced Z-DNA stabilization is coincident with the Hofmeister series, we characterized DNA denaturing capabilities, one of Hofmeister effect on double-stranded DNA (dsDNA) [25,26], with various salts. To do that, we prepared a short random DNA duplex, named B_{12bp}, and Cy3 (donor) and Cy5 (acceptor) dyes were labeled at the same ends of the duplex as a FRET probe to report the degree of DNA denaturation [Fig. 2.6(a)]. To measure the degree of denaturation, bulk FRET measurements was used. It was exhibited a clear ion-concentration dependent phase transitions from a high FRET state to a low FRET state [Fig. 2.6(b)]. Low FRET state was confirmed as denaturation of dsDNA with single-molecule FRET experiment (Fig. 2.7). We repeated this bulk experiment with various salt and from these results the degree of helix-to-coil transition with various salts was obtained [Fig. 2.6(c)]. By comparison with Fig. 2.4(d) and Fig. 2.6(c), (ClO_4^-) and (Ca^{2+}) is more efficient than (Cl^-) and (Mg^{2+}) in both B-to-Z transition and denaturation, respectively. Therefore, the correlation between two transitions is clear at least these cases.

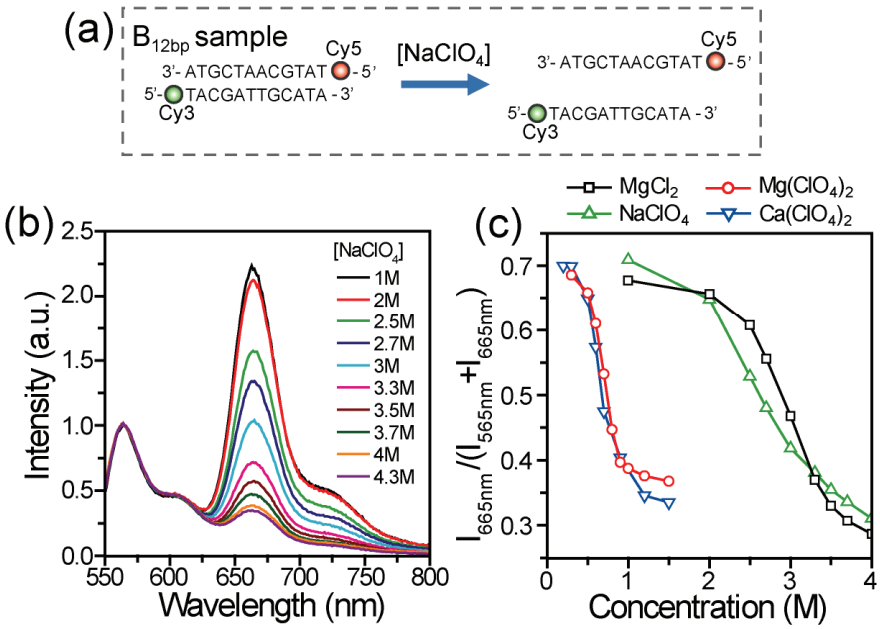

Figure 2.6. DNA denaturation by various salts. (a) DNA sequences, named B_{12bp}, for single-molecule and bulk FRET studies. (b) Fluorescence spectra of B_{12bp} at various $NaClO_4$ concentrations. (c) Bulk FRET was used to quantify the degree of DNA denaturation at various salt conditions. In the graphs, Ipeak means fluorescence intensity at peak designated. Experiments were done at 28 ℃.

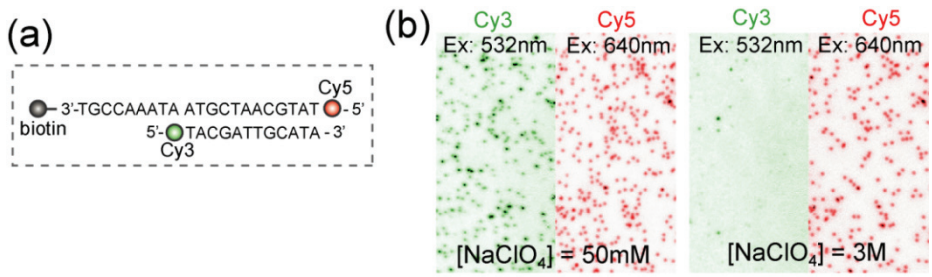

Figure 2.7. Observation of DNA denaturing at high salt concentrations via single-molecule FRET experiment. (a) DNA sample for single-molecule FRET experiment. (b) DNA sample for denaturing experiment Single-molecules images of DNA. Donor (Cy3) was excited under green (532nm) laser, whereas acceptor (Cy5) was activated under red (640nm) laser. At 50 mM of $NaClO_4$, DNA samples were immobilized on the surface and well separated. However, after injecting 3M of $NaClO_4$, Cy3 signals appeared due to denaturation of duplex DNA but Cy5 signals was observed due to immobilization. Images were obtained after 10 minutes.

2.3.3. Generality of Hofmeister series in B-to-Z transition

The conclusion is more clearly visualized in the correlation plot of the midpoints of B-to-Z transitions and denaturation (Fig. 2.8). Furthermore, Fig. 2.8 shows that this correlation is valid in a DNA duplex with six consecutive CG having one BZ junction and no junction, named $B(CG)_6$ and $(CG)_6$, respectively (sequences are in Table 2.1). Z-DNA fraction was quantified with various salts by using single molecule FRET or CD measurements (Fig. 2.9 and 2.10); in case of $(CG)_6$ sample, single-molecule FRET could not be used because BZ transition was not detectable (Fig. 2.11). As shown in Fig. 2.8, the results of this study are summarized: a relative distribution of denaturing midpoints of B_{12bp} and BZ transition midpoints of $(CG)_6$ (black squares), $B(CG)_6$ (red circles), and $B(CG)_6B$ (blue triangles) for various salts. It is clear that the Z-DNA inducing capability of a salt is generally determined by its DNA denaturing capability and generality of Hofmeister effect on BZ transition is maintained with or without BZ junctions.

In addition to that, we notice a few interesting observations from Fig. 2.8. First, the existence of BZ junction increases the BZ transition midpoints, suggesting that base flipping process requires more concentrated salt than the BZ transition of the CG repeat. Second, in the presence of BZ junction, BZ transition was observed only in salts with the most chaotropic anions such as ClO_4^- and I^-, suggesting that anion effect is more dominant in base flipping process than in the BZ transition of the CG repeat. For example, $MgCl_2$ is more efficient than $NaClO_4$ in inducing B-Z transition with $(CG)_6$ DNA, but

$MgCl_2$ is not able to induce Z-DNA with $B(CG)_6$ and $B(CG)_6B$ at all, whereas $NaClO_4$ is able to. And third, divalent cations are generally more efficient in inducing Z-DNAs than monovalent cations—the salts with divalent cations are positioned lower than the guiding black dashed line in Fig. 2.8, but the salts with monovalent cations are positioned above the line.

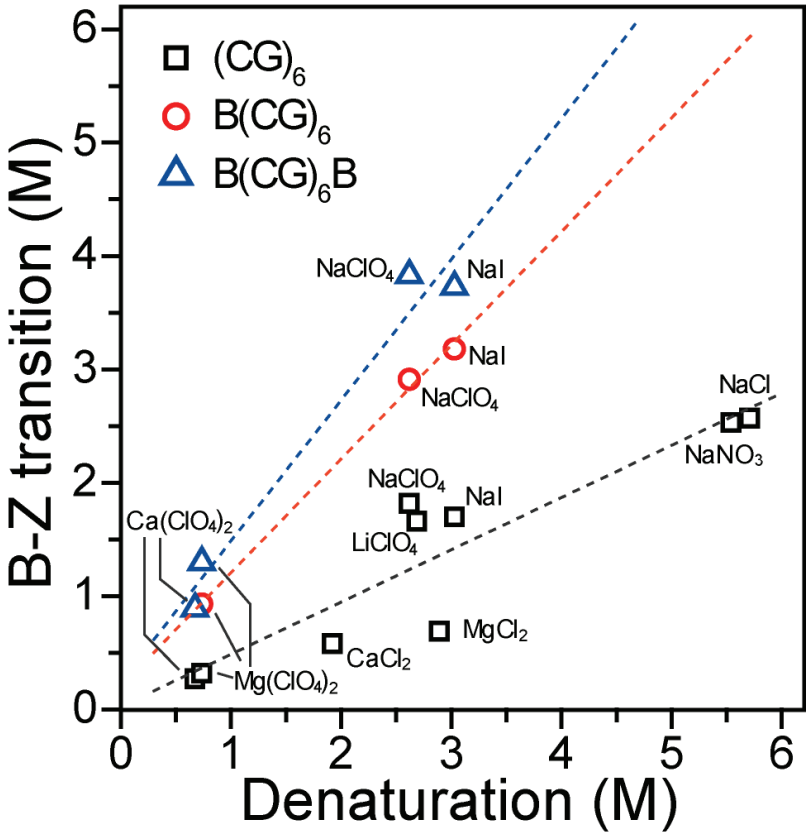

Figure 2.8. Junction effect on BZ transition. Relative distribution of denaturation midpoints of B_{12bp} and BZ transition midpoints of $(CG)_6$ (black squares), $B(CG)_6$ (red circles), and $B(CG)_6B$ (blue trangles) for designated salts.

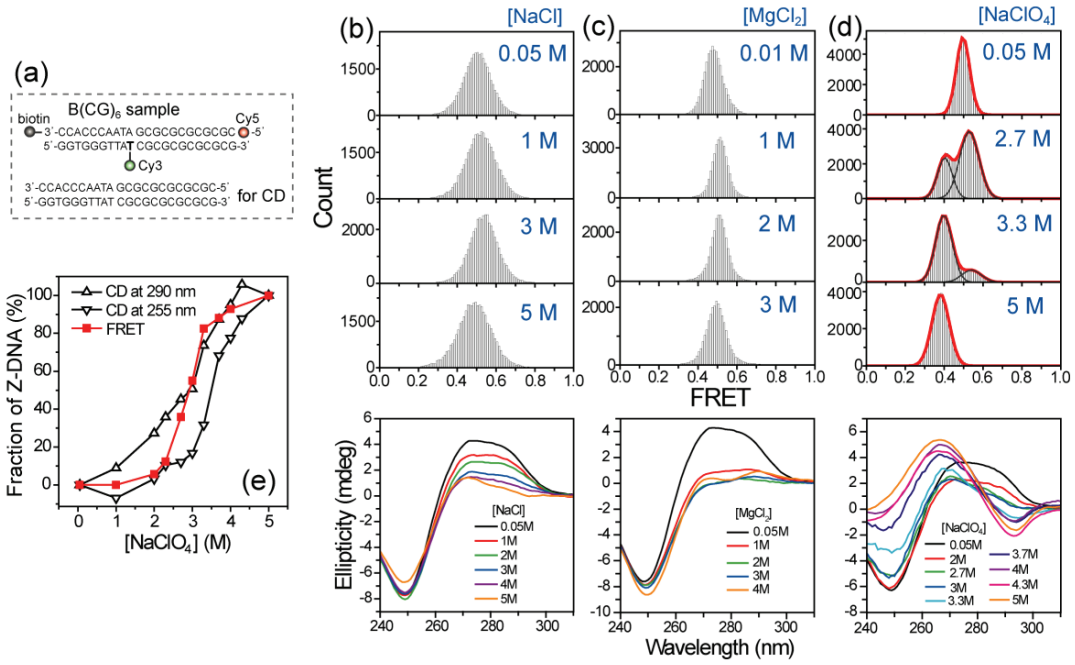

Figure 2.9. Titration of $B(CG)_6$ DNA sample at various salt condition. (a) DNA sequences of $B(CG)_6$. For CD measurement, non-modified DNA sample was used. (b) – (d) FRET histograms and CD spectra of $B(CG)_6$ at various NaCl, $MgCl_2$, and $NaClO_4$ concentrations, respectively. (e) Fraction of Z-DNA was calculated from single-molecule measurements (red squares), and CD measurements at 255-nm (lower triangles), and at 290-nm (upper triangles) was obtained from CD spectra of (d). Fraction of Z-DNA calculated from CD measurements at 255-nm and at 290-nm was not same each other, i.e. the CD signal is not a simple linear sum of B-form and Z-form. In conclusion, single-molecule FRET approach is more accurate in Z-DNA quantity.

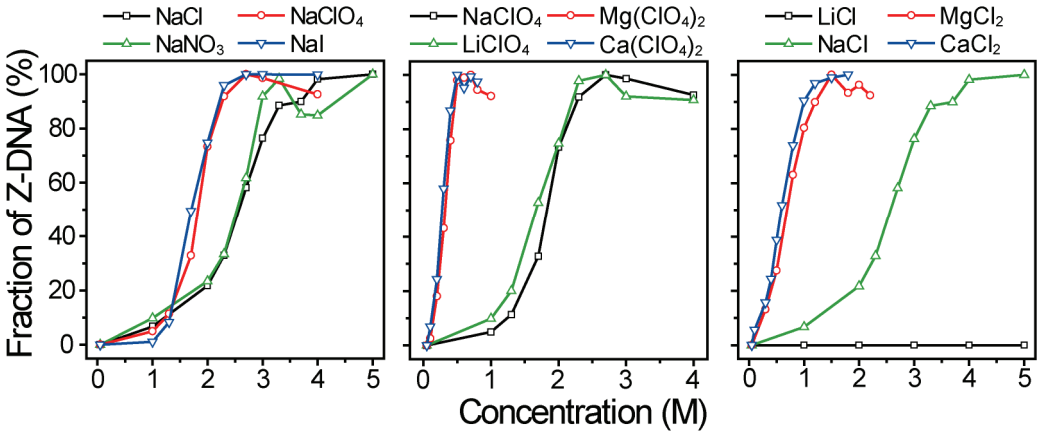

Figure 2.10. Salt-induced BZ transition of $(CG)_6$. CD spectra of $(CG)_6$ at various salt conditions. All experiments were done at 25 ^{o}C.

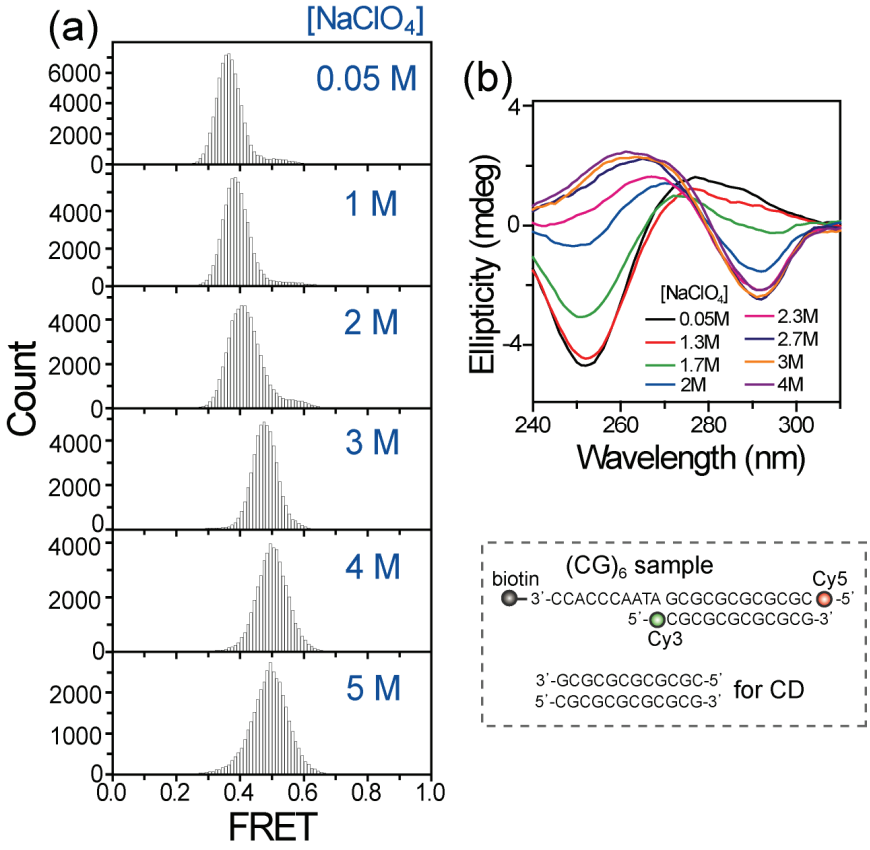

Figure 2.11. Comparison of single-molecule FRET and CD with $(CG)_6$. (a) Single-molecule FRET histograms of $(CG)_6$ at various $NaClO_4$ concentrations. Except a gradual FRET increase, no low FRET peak emerged at high salt conditions. (b) CD spectra of $(CG)_6$ at various $NaClO_4$ concentration. BZ transition is clear in CD measurements. The DNA sequences are shown at the bottom.

2.4. Discussions

In discussion, this discovery reported in this letter is not just a simple addition to the Hofmeister phenomena already ubiquitous, but also have implications for the following controversies. First, the correlation between denaturing capabilities and Z-DNA-inducing capabilities gives insight to answer the chain sense paradox of BZ transition [13,27]. The conformational change from B-DNA to Z-DNA is accompanied by the overturning of all the base pairs as well as the change of helix direction, right-handed to left-handed. Attributable to the lack of rotating spaces of each base pairs, there are different argues that the length of DNA become longer enough to rotate (the expand-rotate-collapse model), or base pairs instantly break out and rotate then make base pairs again (the sequential-hydrogen-bond-breaking model). Our observation support the sequential-hydrogen-bond-breaking model rather than the expand-rotate-collapse model because structure breaking effect by chaotropic ions is thought to help base pairs break.

And second, it may have an implication for the mechanism of the Hofmeister phenomena itself. Since Franz Hofmeister first classified various ions in the order of their salting out and salting in abilities, so called the Hofmeister series [27], it has been reported that the series is valid in quite a broad range of phenomena including enzyme activities, protein stability, surface tension, micelle formation, and bacterial growth [22]. However, the molecular mechanism of the Hofmeister effects is still unclear. Initially it was

proposed that salts influence molecular interactions by making or breaking bulk water structures [23, 24]. However, recent studies found that the hydrogen-bonding network of water molecules was not significantly disturbed by ions [27], and an alternative model that direct ion–macromolecule interactions cause the Hofmeister effects is gaining a momentum [28].

In this study, we used single-molecule FRET to accurately quantify Z-DNA populations at various salt conditions. Interestingly, our data suggested that formation of Z-DNA is dependent on the Hofmeister effect of salts, which is somewhat contradictory to the well-accepted explanation that based on the electrostatic screening of cations. Since the Hofmeister effect of salts on Z-DNA formation may rely on anion species, an intriguing question arises: how can anions directly interact with negatively charged DNAs as proposed in the currently popular model of the Hofmeister effects? Further studies to understand the exact mechanism of B-to-Z transition is expected to provide an insight into the Hofmeister effect of salts *per se*.

2.5. References

[1] A. Rich, *Gene* **1993**, 135, 99-109.

[2] R. D. Wells, *Trends Biochem. Sci.* **2007**, 32, 271-278.

[3] J. Choi, T. Majima, *Chem. Soc Rev.* **2011**, 40, 5893-5909.

[4] A. H. Wang, G. J. Quigley, F. J. Kolpak, J. L. Crawford, J. H. van Boom, G. van der Marel, A. Rich, *Nature* **1979**, 282, 680-686.

[5] F. M. Pohl, T. M. Jovin, *J. Mol. Biol.* **1972**, 67, 375-396.

[6] A. Rich, A. Nordheim, A. H. Wang, *Ann. Rev. Biochem.* **1984**, 53, 791-846.

[7] A. Rich, S. Zhang, *Nat. Rev. Genet.* **2003**, 4, 566-572.

[8] B. Wittig, S. Wolfl, T. Dorbic, W. Vahrson, A. Rich, *EMBO J.* **1992**, 11, 4653-4663.

[9] A. Herbert, K. Lowenhaupt, J. Spitzner, A. Rich, *Proc. Natl. Acad. Sci. USA* **1995**, 92, 7550-7554.

[10] R. Liu, H. Liu, X. Chen, M. Kirby, P. O. Brown, K. Zhao, *Cell* **2001**, 106, 309-318.

[11] H. Liu, N. Mulholland, H. Fu, K. Zhao, *Mol. Cell. Biol.* **2006**, 26, 2550-2559.

[12] G. Wang, S. Carbajal, J. Vijg, J. DiGiovanni, K. M. Vasquez, *J. Natl. Cancer I.* **2008**, 100, 1815-1817.

[13] M. A. Fuertes, V. Cepeda, C. Alonso, J. M. Perez, *Chem. Rev.* **2006**, 106, 2045-2064.

[14] M. Behe, G. Felsenfeld, *Proc. Natl. Acad. Sci. USA* **1981**, 78, 1619-1623.

[15] D. M. Soumpasis, M. Robert-Nicoud, T. M. Jovin, *FEBS Lett.* **1987**, 213, 341-344.

[16] T. F. Kagawa, M. L. Howell, K. Tseng, P. S. Ho, *Nucl. Acids Res.* **1993**, 21, 5978-5986.

[17] T. Ha, T. Enderle, D. F. Ogletree, D. S. Chemla, P. R. Selvin, S. Weiss, *Proc. Natl. Acad. Sci. USA* **1996**, 93, 6264-6268.

[18] F. Hofmeister, *Arch. Exp. Pathol. Pharmakol.* **1888**, 24, 247-260.

[19] P. H. Vonhippel, K. Y. Wong, *Science* **1964**, 145, 577-580.

[20] M. G. Cacace, E. M. Landau, J. J. Ramsden, *Q. Rev. Biophys.* **1997**, 30, 241-277.

[21] Y. Zhang, P. S. Cremer, *Annu. Rev. Phys. Chem.* **2010**, 61, 63-83.

[22] S. C. Ha, K. Lowenhaupt, A. Rich, Y. G. Kim, K. K. Kim, *Nature* **2005**, 437, 1183-1186.

[23] S. Bae, D. Kim, K. K. Kim, Y. G. Kim, S. Hohng, *J. Am. Chem. Soc.* **2011**, 133, 668-671.

[24] R. Roy, S. Hohng, T. Ha, *Nat. Methods* **2008**, 5, 507-516.

[25] K. Hamaguchi, E. P. Geiduschek, *J. Am. Chem. Soc.* **1962**, 84, 1329–1338.

[26] L. M. Pegram, T. Wendorff, R. Erdmann, I. Shkel, D. Bellissimo, D. J. Felitsky, M. T. Record, *Proc. Natl. Acad. Sci. USA* **2010**, 107, 7716-7721.

[27] S. C. Harvey *Nucl. Acids Res.* **1983**, 11, 4867-4878.

[28] A. W. Omta, M. F. Kropman, S. Woutersen, H. J. Bakker, *Science* **2003**, 301, 347-349.

[29] Y. Zhang, P. S. Cremer, *Curr. Opin. Chem. Biol.* **2006**, 10, 658-663.

Chapter 3. Energetic information of Z-DNA at high salt concentration

3.1. Introduction

DNA is a dynamic molecule whose conformation is interconverted between diverse isoforms spontaneously such as DNA-triplex, G-quadruplexes, kink, i-motif, and Z-DNA [1,2]. Among these non-canonical conformations, Z-DNA is quite drastic changed one whose helical structure is left handed with a zigzag backbone [3]. While it is rarely formed with a very brief lifetime under normal conditions, Z-DNA becomes dominant with various factors such as high ionic concentrations, negative supercoiling, chemical modifications of bases, and Z-DNA binding proteins [4-6]. Initially Z-DNA formation was observed at high salt concentrations, registering a salt as the first-discovered Z-DNA inducing factor [7]. And Z-DNA crystal structure [3] was revealed that the bases of Z-DNA has repetitive syn- and anti-conformations in contrast to the bases of B-DNA which has only anti-conformation. Therefore Z-DNA prefer alternating purine/pyrimidine residues because purines is easier to have syn-conformation than pyrimidines.

Recently the driving force of B-to-Z transition at high ionic concentration was revealed to that Hofmeister (ion specific) effect of salt, not simple coulombic (nonspecific) effect. Although the origin of B-to-Z transition by high ionic concentration was understood, the energetic information was not

obtained completely. Especially the change of energy was limited to understand when number of BZ junction or CG repeats was different. In ensemble studies, measurement of Z-DNA fraction was limited due to the little portion of change when BZ junction was added [8]. To address this question, we employed single-molecule Fluorescence Resonance Energy Transfer (smFRET) technique [9] along with circular dichroism (CD) measurements.

In previous study, we were successful to distinguish between B-DNA and Z-DNA using by smFRET in single-molecule level [10]. For smFRET study, DNA sample was immobilized on poly-ethylene glycol coated quartz surface by streptavidin-biotin interaction [Fig. 1(a)]. And images were obtained in a homemade wide-field total-internal-reflection fluorescence (TIRF) microscope using an electron multiplying charge-coupled device (EM-CCD).

3.2. Results

3.2.1. BZ transition of various DNA samples

To characterize Z-DNA formation via single-molecule FRET [Fig.3.1(a)] with different DNA samples, we prepared various DNA samples which has repetitive Cytosine-Guanine bases with or without BZ junction at the end of each side [six- repetitive CGs only sample – named $(CG)_6$, six CGs with one junction – named $B(CG)_6$, six CGs with two junctions – named $B(CG)_6B$, and eight CGs with two junctions – named $B(CG)_8B$]. And we attached donor and acceptor dye at BZ junction region to maximize FRET change as shown in Fig. 3.1(b).

In the first place, we performed titration experiment using by single-molecule FRET to obtain Z-DNA fraction as the concentration of sodium perchlorate on our various samples. As a result, we were able to distinguish B- and Z-DNA from FRET value and obtained FRET histogram of $B(CG)_8B$ sample as the concentration of sodium perchlorate. As shown in Fig. 3.2(a), low FRET peak near 0.2 value which was considered to Z-DNA appeared as increase of salt concentration and became a dominant state more than 3.7M sodium perchlorate concentration. It was also confirmed with CD measurements that B-to-Z transition occurred in similar salt concentration (Fig. 3.3). From these histograms, Z-DNA fraction was obtained directly. As shown in Fig. 3.2(b), Z-DNA fraction on sodium perchrolate of our tested samples were summarized. In this figure, only $(CG)_6$ sample was obtained from CD data and the others were from FRET histograms. Some interesting

factors was seen in this Figure. First, the data were looked as sigmoidal curve. And as BZ junctions was added, more sodium perchlorate concentration was needed for B-to-Z transition. Contrary to $(CG)_6$ sample, midpoint of $B(CG)_6$ was higher and midpoint of $B(CG)_6B$ was higher than it of $B(CG)_6$, suggesting that BZ junction had a role to hinder B-to-Z transition. On the other hand, (CG) repeat help B-to-Z transition. Midpoint of $B(CG)_8B$ sample was lower that it of $B(CG)_6B$ sample and also, midpoint of $(CG)_6$ was lower than that of $(CG)_3$ [Fig. 3.2(c)].

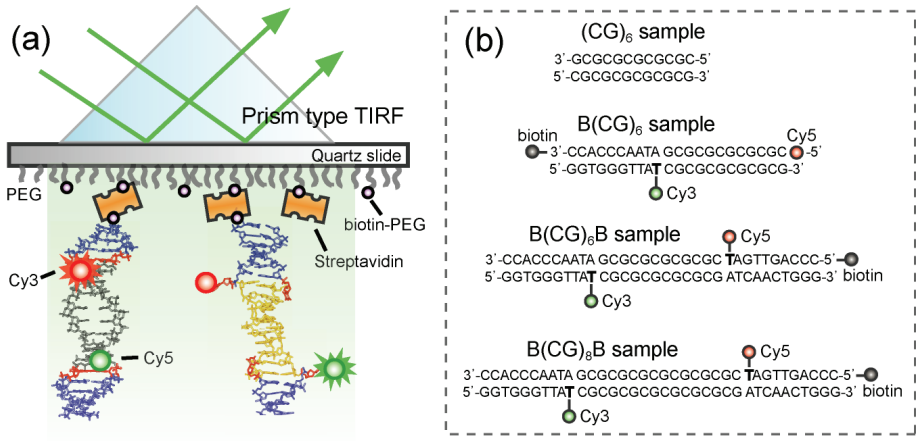

Figure 3.1. Single-molecule FRET (smFRET) assay and DNA samples. (a) A schematic diagram of total-internal-reflection fluorescence (TIRF) microscope. DNA sample was immobilized on quartz surface by biotin-streptavidin interaction. CG-repeat was colored to gray (B-form) or yellow (Z-form), random sequences were colored to blue, and flipping region in Z-DNA or dye attached region were colored to red. (b) DNA samples prepared. In case of $(CG)_6$, smFRET could not be used due to impossibility of detecting BZ transition but in the others, smFRET could be used.

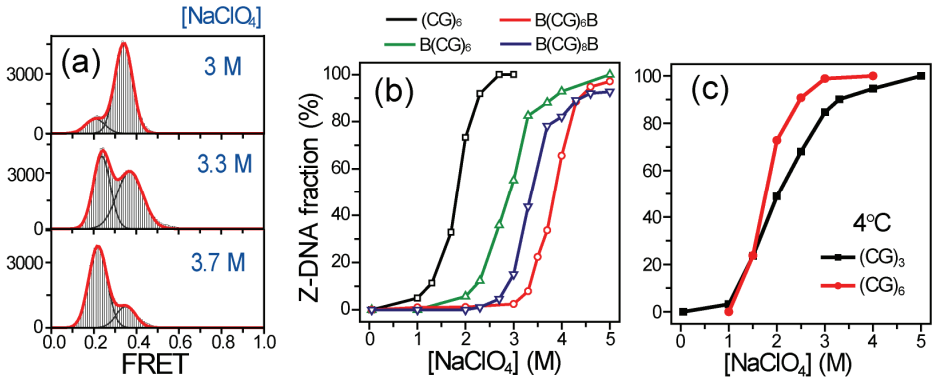

Figure 3.2. (a) FRET histograms of $B(CG)_8B$ at various $NaClO_4$ concentrations. Low FRET value near 0.2 means Z-DNA. (b) Z-DNA fraction of our various DNA samples as $NaClO_4$ concentrations. Only $(CG)_6$ sample was obtained from CD data and the others were from FRET histograms. (c) Z-DNA fraction of $(CG)_3$ and $(CG)_6$.

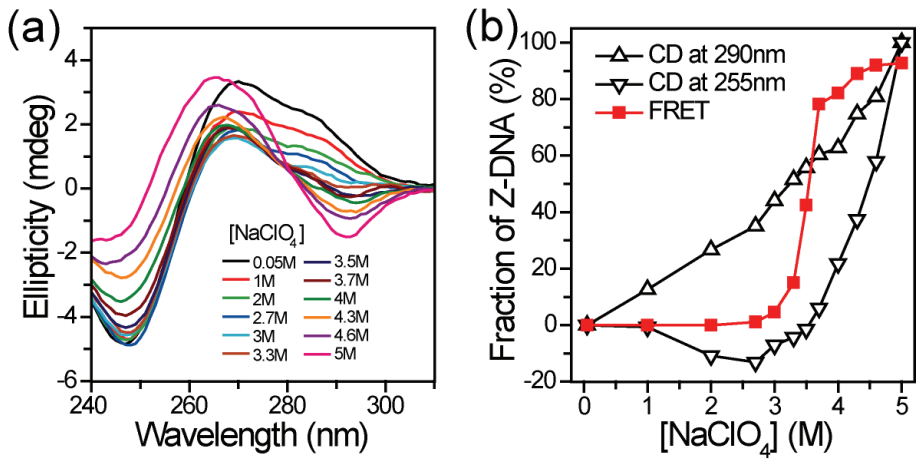

Figure 3.3. CD data with $B(CG)_8B$ sample. (a) CD spectra of $B(CG)_8B$ as a function of $NaClO_4$ concentrations. (b) Z-DNA fraction was calculated from single-molecule measurements [red squares, Fig 3.2(a)], and CD measurement at 255-nm (lower triangles), and at 290-nm (upper triangles) from (a). B-to-Z transition occurred at similar $NaClO_4$ concentration.

3.2.2. Energetics for junction, (CG) repeats

To obtain energetic information, we selected 3.3M sodium perchlorate concentration where both B-DNA and Z-DNA were measured in all of our samples. And we carried out temperature dependence experiments with all samples. As a result, in case of $(CG)_6$ sample, Z-DNA fraction was decreased as increase of temperature compatible to previous study as shown in Fig. 3.4(a). It was strikingly of interest, however, that Z-DNA fraction was somewhat increased as increase of temperature when BZ junction was added [Fig. 3.4(b) and Fig. 3.5].

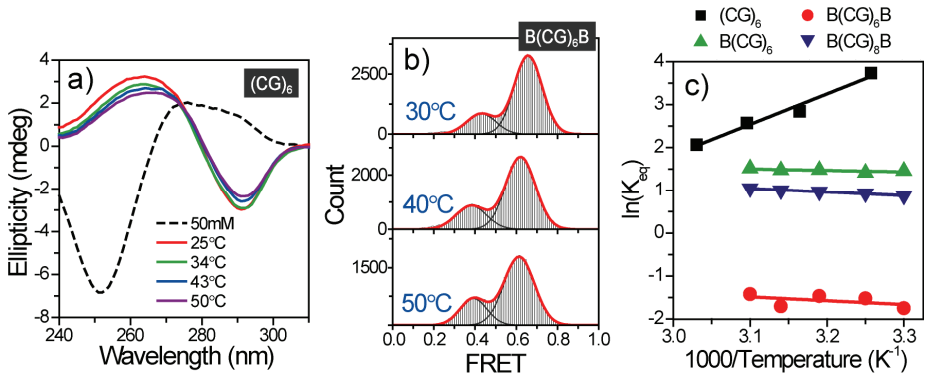

Figure 3.4. Temperature dependence of various samples on 3.3N $NaClO_4$ concentration. (a) CD spectra of $(CG)_6$ at different temperature. Increase at 255nm or decrease at 290nm than spectrum of 0.05M $NaClO_4$ concentration means decrease of Z-DNA fraction. (b) FRET histogram of $B(CG)_6B$ sample at designated temperature. Low FRET value near 0.4 means Z-DNA fraction. (c) Natural logarithm of equilibrium constant versus temperature with various samples yield the standard state enthalpy and entropy from equation (3.1).

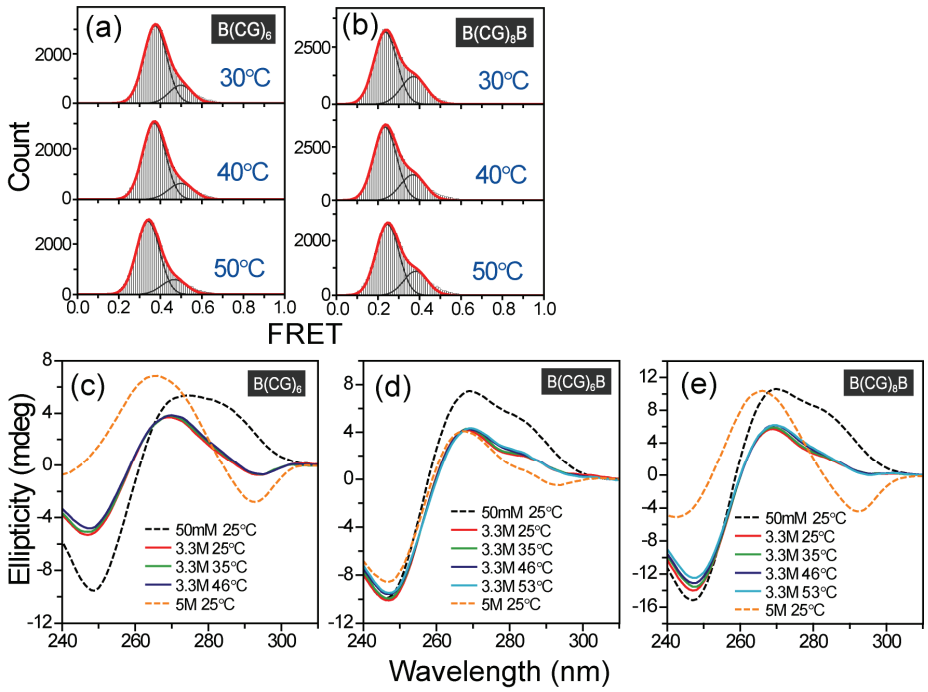

Figure 3.5. Temperature dependence of various samples. (a) and (b) FRET histogram at different temperature of $B(CG)_6$ and $B(CG)_8B$ samples from single-molecule FRET measurement, respectively. (c)-(e) Temperature dependence of $B(CG)_6$, $B(CG)_6B$, and $B(CG)_6B$ samples from CD measurement, respectively. Similar to FRET histogram, Z-DNA fraction is somewhat increased at higher temperature.

To determine the effect of Enthalpy and Entropy, we extracted enthalpic and entropic value by fitting with van't Hoff equation,

(3.1) $\ln(K_{eq}) = \frac{\Delta S^{o}_{B-to-Z}}{R} - \frac{1}{T}\frac{\Delta H^{o}_{B-to-Z}}{R}$

, where R is the ideal gas constant. From this equation, a linear fit was done for all samples as shown in Fig. 3.4(c) and enthalpic and entropic information was obtained (Table 3.1).

Table 3.1. Thermodynamic parameters at 3.3M $NaClO_4$ (25 ^{o}C)

	ΔH^{o}_{B-to-Z} (kcal/mol)	ΔS^{o}_{B-to-Z} (cal/mol/K)	ΔG^{o}_{B-to-Z} (kcal/mol)
$(CG)_6$	-14.1	-38.6	-2.6
$B(CG)_6$	0.68	2.5	-0.07
$B(CG)_6B$	1.77	5.1	0.25
$B(CG)_8B$	1.66	7.2	-0.49

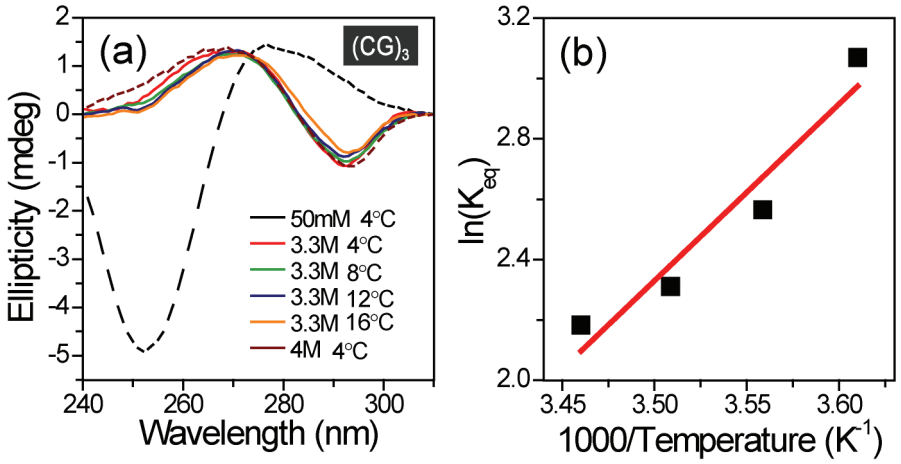

Figure 3.6. Temperature dependence of $(CG)_3$ sample. (a) CD data of $(CG)_3$ at various temperature. As temperature increased, Z-DNA fraction were decreased. (b) Natural logarithm of equilibrium constant versus temperature.

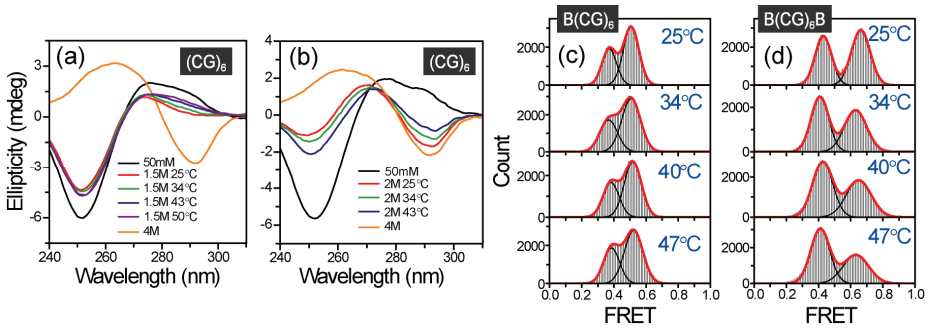

Figure 3.7. Temperature of various DNA samples at different $NaClO_4$ concentration conditions. (a) and (b) CD data of $(CG)_6$ sample at different $NaClO_4$ concentration designated at various temperature. (c) and (d) FRET histogram of $B(CG)_6$ and $B(CG)_6B$ sample at 2.7M and 3.7M $NaClO_4$ concentration at designated temperature, respectively.

3.3. Discussions

In discussion, enthalpic and entropic term were competed each other to make Z-DNA and interestingly role of enthalpy and entropy was different whether BZ junction was added or no. In case of $(CG)_6$, enthalpic term help B-to-Z transition but entropic term hinder this change. Similar result was observed to different repetitive CGs, $(CG)_3$ (Fig. 3.6). However, when BZ junction was added, the situation was changed entirely so that entropic term helped B-to-Z transition and enthalpic term hinder this transition. Therefore, the driving force of B-to-Z transition was enthalpy without BZ junctions but it was changed to entropy when any BZ junctions were added. These results were also observed at different sodium perchlorate concentrations (Fig. 3.7).

In summary, we measured B-to-Z transition by high salt concentration with or without BZ junction using by single-molecule FRET technique along with circular dichroism measurement. As a result, BZ junction or number of CGs affect B-to-Z transition in many aspects. First, midpoint of B-to-Z transition by salt became higher as adding BZ junction but lower as number of CGs. And second, when BZ junction was added, sign of enthalpic and entropic energy difference between B-DNA and Z-DNA was converted in whole.

3.4. References

[1] A. Rich, *Gene* **1993**, 135, 99-109.

[2] J. Choi and T. Majima, *Chem. Soc Rev.* **2001**, 40, 5893-5909.

[3] A. H.-J. Wang, G. J. Quigley, F. J. Kolpak, J. L. Crawford, J. H. van Boom, G. van der Marel, A. Rich, *Nature* **1979**, 282, 680-686.

[4] A. Rich, A. Nordheim, A. H. Wang, *Ann. Rev. Biochem.* **1984**, 53, 791-846

[5] A. Rich, S. Zhang, *Nat. Rev. Genet.* **2003**, 4, 566-572.

[6] M. A. Fuertes, V. Cepeda, C. Alonso, J. M. Pérez, *Chem. Rev.* **2006**, 106, 2045-2064.

[7] F. M. Pohl, J. M. Jovin, *J. Mol. Biol.* **1972**, 67, 375-396.

[8] Y. -G. Kim, K. Lowenhaupt, S. Maas, A. Herbert, T. Schwartz, and A. Rich, *J. Biol. Chem.* **2000**, 275, 26828-26833.

[9] T. Ha, Th. Enderle, D. F. Ogletree, D. S. Chemla, P. R. Selvin, S. Weiss, *Proc. Natl. Acad. Sci. USA* **1996**, 93, 6264-6268.

[10] S. Bae, D. Kim, K. K. Kim, Y. -G. Kim, S. Hohng, *J. Am. Chem. Soc.* **2011**, 133, 668-671.

Chapter 4. B-to-Z transition mechanism via Zα protein

4.1. Intruction

Specificity is a premise of life and highly specific interactions are ubiquitous in many biological interactions between protein-DNA, protein-protein, protein-metabolites, etc. The lock-and-key model was proposed to explain the high specificity of molecular recognition by a precise structural fit of interacting molecules. [1]. In most specific interactions, however, the formation of molecular complexes is coupled with small- or large-scale structural rearrangements [2-4]. Two representative mechanisms have been envisioned for the achievement of the final precise fit: in the "induced fit" model, initial binding actively starts the development of the structural change [5], and in the "conformational selection" model, a pre-existing precise fit becomes a dominant structure through a passive but selective stabilization process [6]. Even though it is a fundamental question which pathway is actually used to achieve a final match of many specific molecular interactions, experimental evidences are rare and controversies are still going on [7-12].

The structural transition between right-handed B-DNA [13] and left-handed Z-DNA [14,15], i.e. B-Z transition, is such an example. Left-handed Z-DNA is preferably formed in purine-pyrimidine repeats at extremely high

salt concentrations in vitro [16] or with the help of negative supercoiling in vivo [17]. Alternatively, recent studies revealed that the B-to-Z transition can be also mediated by Z-DNA binding proteins (ZBPs) [18-21], providing a good model system to answer the compelling question whether the proteins actively induce Z-DNAs or passively trap preformed Z-DNAs [22]. A conceivable way to most directly answer the question is to study the ZBP's effect on intrinsic B-Z transition dynamics, if there is any. Recently, fluorescence resonance energy transfer (FRET) assays [23,24] were developed to detect salt- or supercoiling-induced B-Z transitions at single-molecule level [25]. In this work, we applied single-molecule FRET technique to observe real-time dynamics of intrinsic B-Z transition at low-salt and relaxed conditions, ZBP binding/dissociation events, and accompanying B-to-Z transitions.

4.2. Materials and Methods

4.2.1. Sample preparation

Proteins were prepared as described. For single-molecule FRET measurements, the following DNA strands were purchased from Integrated DNA Technologies (Coralville, IA):

5'-GGTGGGTTAT/iAmC6/CGCGCGCGCGCG-3',

5'-/Cy5/CGCGCGCGCGCG ATAACCCACC/biotin/-3'.

The amine-modified T (T/iAmC6/) was labelled with Cy3 as described.2 DNA duplex were prepared by mixing the biotinylated and non-biotinylated stand in 1:2 ratio at 50 μM concentration in a buffer containing 10mM Tris (pH 8.0) and 50mM NaCl. The non-biotinylated strand was added in excess to minimize the chance of having un-annealed biotinylated strand in the measurement. The annealing mixture was heated at 95 ºC for 3 minutes and allowed to cool down slowly for 1.5 hours in a heating block. The annealed DNA duplex contains 6 CG repeats at one end, which can make transitions from B-form to Z-form, and *vice versa*.

4.2.2. Experimental methods

Single-molecule FRET measurements. A quartz slide was coated with poly-ethylene glycol (PEG) and streptavidin as described [24]. After immobilizing biotinylated DNA (80 pM), images were obtained in a wide-field total-internal-reflection fluorescence microscope with 100-ms time resolution using an electron multiplying charge-coupled device (EM-CCD) camera (iXon DV887ECS-BV, Andor Technology) and a homemade C++ program. Measurements were performed at 25 ºC for Figure 1 and 3, or at 37 ºC for Figure 2 with the following buffer composition: 10 mM Tris-HCl (pH 8.0), 50 mM NaCl, and an oxygen scavenger system to slow photobleaching.2

Circular Dichroism. CD spectra were recorded using by a Jasco-815 spectropolarimeter through using a quarts cell with an optical path length of

1mm in the wavelength range of 240~310 nm at 25 ℃; the band width 1 nm, the scanning speed 50 nm/min and the response time 8s. For CD measurement, not to be affected by any modification, label-free single stranded DNA (5'-GGTGGGTTATCGCGCGCGCGCG-3', and 5'-CGCGCGCGCGCGATAACCCACC-3'.) were perchased from Bioneer (Korea) and HPLC purified. DNA duplex were annealed by mixing in 1:1 ratio at 500 μM and were diluted into 5 or 15 μM by 10 mM Tris (pH 8.0) and 50 mM NaCl. For the control of CD experiment, Peltier temperature control accessory was used.

4.3. Results and Discussions

4.3.1. Stepwise B-to-Z transitions occur with time delays after Zα binding

For single-molecule FRET experiments, we prepared dye-labeled DNA duplexes comprising a CG-repeat [gray and yellow in Fig. 4.1(a)] and a flanking random sequence [blue in Fig. 4.1(a)] by annealing the following DNA strands: 5'-/Cy5/CGCGCGCG CGCGATAACCCACC/biotin/-3', and 5'-GGTGGGTTATCy3CG CGCGCGCGCG-3'. The thymine base at the B-Z junction [red in Fig. 4.1(a)], which is flipped out in Z-form [26], was selected as the labeling position of the donor (Cy3) to maximize FRET change during B-to-Z transition. Annealed DNA molecules were immobilized on a polymer-coated quartz surface by biotin-streptavidin interaction, and fluorescence

signals of donor and acceptor were obtained in a wide-field total-internal-reflection fluorescence microscope [Fig. 4.1(a)] [24].

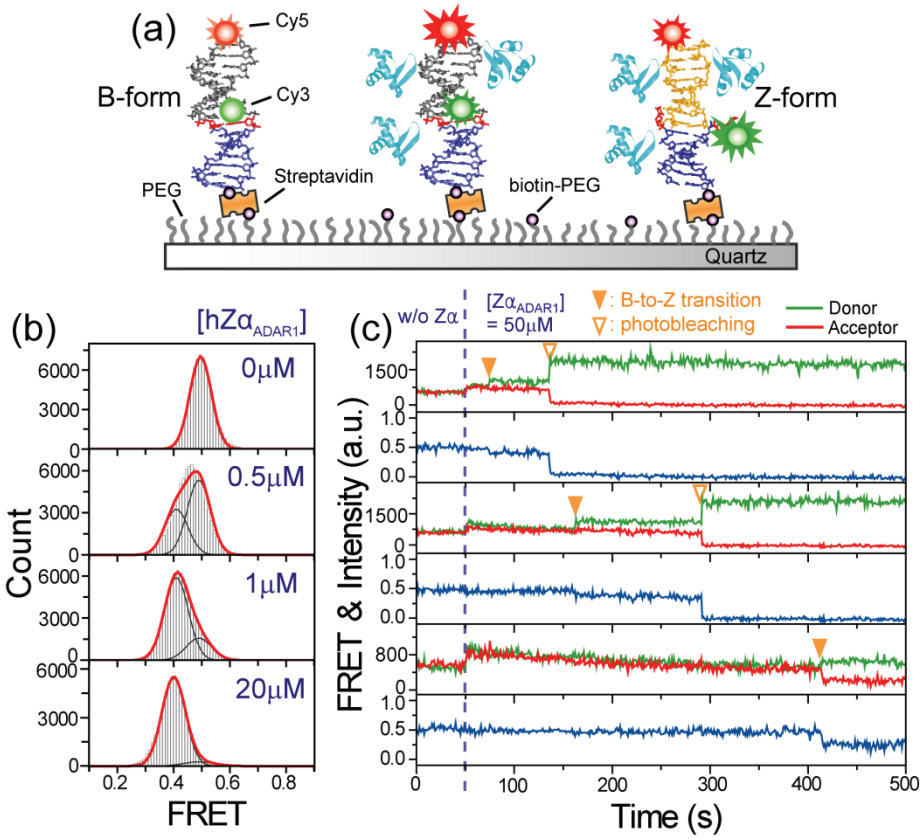

Figure 4.1. Stepwise but delayed protein-induced B-to-Z transition. (a) Experimental scheme. DNA duplex comprising a random sequence region (blue), and a flanking CG repeat, were immobilized on polymer-coated quartz surface by biotin-streptavidin interaction. As the CG repeat switches between B-form (gray) and Z-form (yellow), simultaneous FRET fluctuation is expected. (b) FRET histograms at various hZα$_{ADAR1}$ concentrations (T = 25 ^{o}C). (c) Buffer exchange experiments. At 50 s (blue dashed line), 50 μM

$hZ\alpha_{ADAR1}$ was rapidly delivered into a detection chamber. Instantaneous intensity increase of donor (green lines) and acceptor (red lines) indicates that binding equilibrium of Zα proteins is established fast (< 1s). FRET transitions (solid triangles) occur with time delays in a stepwise manner. Open triangles indicate photobleaching of acceptors.

First, we studied B-Z transition initiated by the binding of the Zα domain of human double stranded RNA adenosine deaminase ($hZ\alpha_{ADAR1}$), which is one of the most efficient Z-DNA-inducing proteins with a wealth of biochemical and structural information on it. Fig. 4.1(b) shows FRET histograms of the DNA duplexes after 30-minute incubation with various concentrations of $hZ\alpha_{ADAR1}$. In the absence of $hZ\alpha_{ADAR1}$, FRET histogram was well fitted by a single Gaussian distribution, confirming the existence of single-conformation, i.e. B-DNA. Above 0.5 μM $hZ\alpha_{ADAR1}$ concentration, however, low FRET peak started to appear and became a dominant state at higher protein concentrations. Circular dichroism measurements confirmed that B-to-Z transition actually occurs in this sample with the addition of $hZ\alpha_{ADAR1}$ (Fig. 4.2). In contrast, the experiments with a random DNA duplex (Fig. 4.3) as negative controls did not show such a low FRET state, identifying the low FRET peak in Fig. 4.1(b) as Z-DNA.

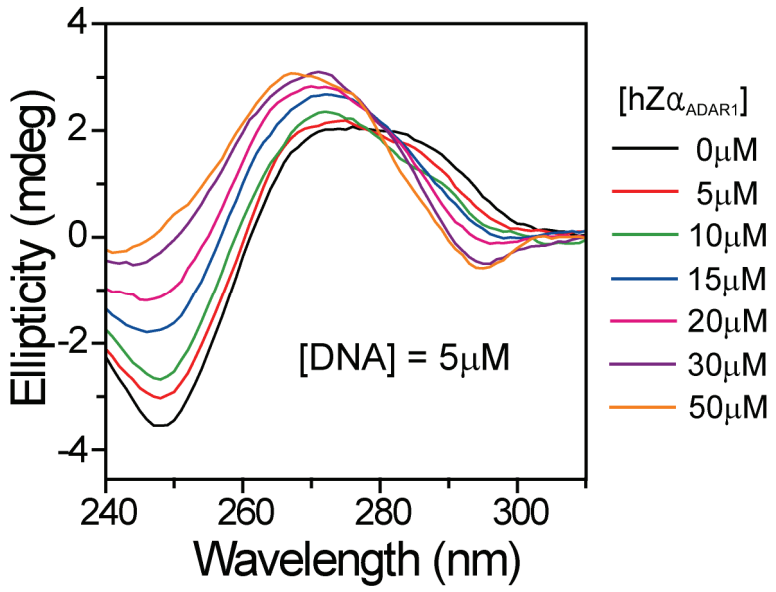

Figure 4.2. CD spectra of a DNA duplex with the same sequence as in Figure 1 at various hZα$_{ADAR1}$ concentrations. DNA concentration was 5 μM, and the experiments were performed at 25 ^{o}C. Both the sign inversion at 290 nm and signal increase at 255 nm indicate that hZα$_{ADAR1}$ efficiently induces B-to-Z transition [6].

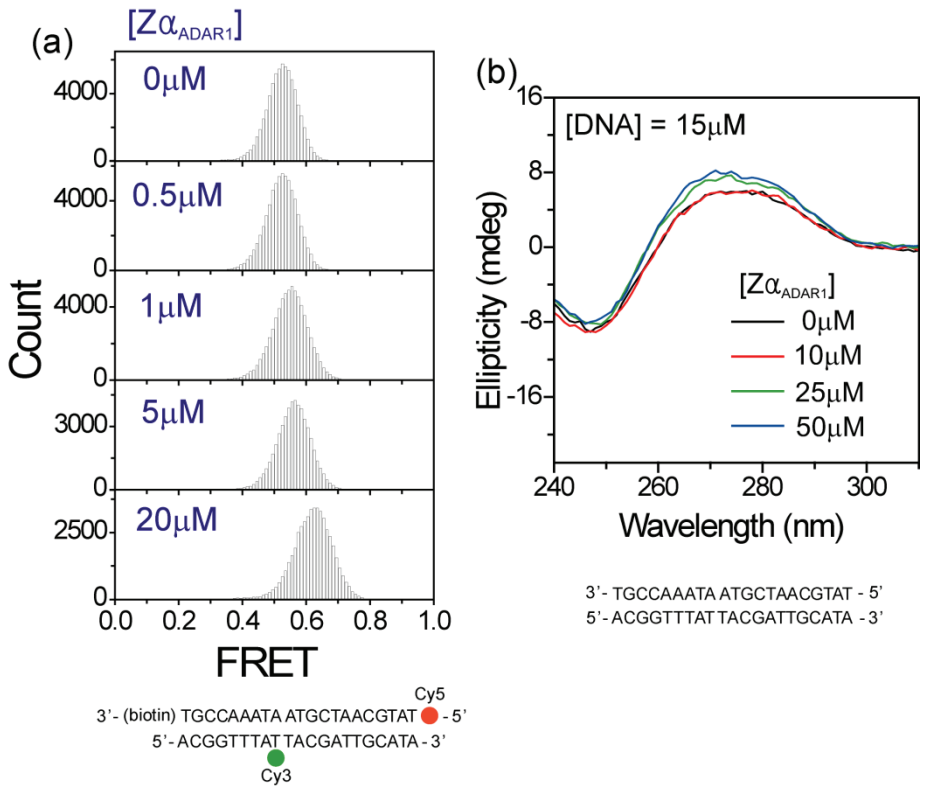

Figure 4.3. Single-molecule FRET and CD experiments on a random DNA duplex. (a) FRET histograms of a random DNA duplex at various $hZ\alpha_{ADAR1}$ concentrations. The DNA sequence and labeling scheme are shown at the bottom. (b) CD spectra of the random duplex at various $hZ\alpha_{ADAR1}$ concentrations. The DNA sequence was the same as in (a) except no labeling in this case. All experiments were performed at 25 ^{o}C. The gradual increase of FRET peak position with increasing protein concentrations in (a) does not accompany a spectral change of CD measurements. Therefore, we speculate that the FRET change occurs due to the protein-dye interaction, not by a structural transition of DNA duplex.

After the successful establishment of a single-molecule monitoring system for the protein-induced B-Z transitions, we investigated details of the B-to-Z transition in the presence of $hZ\alpha_{ADAR1}$. While observing single-molecule fluorescence images of DNA duplexes, we rapidly delivered $hZ\alpha_{ADAR1}$ of saturation concentration (50 μM) into the detection chamber [blue dashed line in Fig. 4.1(c)]. Instantaneous fluorescence-intensity jumps indicated a rapid binding of $hZ\alpha_{ADAR1}$ to DNA duplexes [27]. However, FRET changes corresponding to B-to-Z transitions [orange triangles in Fig. 1(c)] occurred in a stepwise manner with long time delays (5.4 minute average transition time, Fig. 4.4).

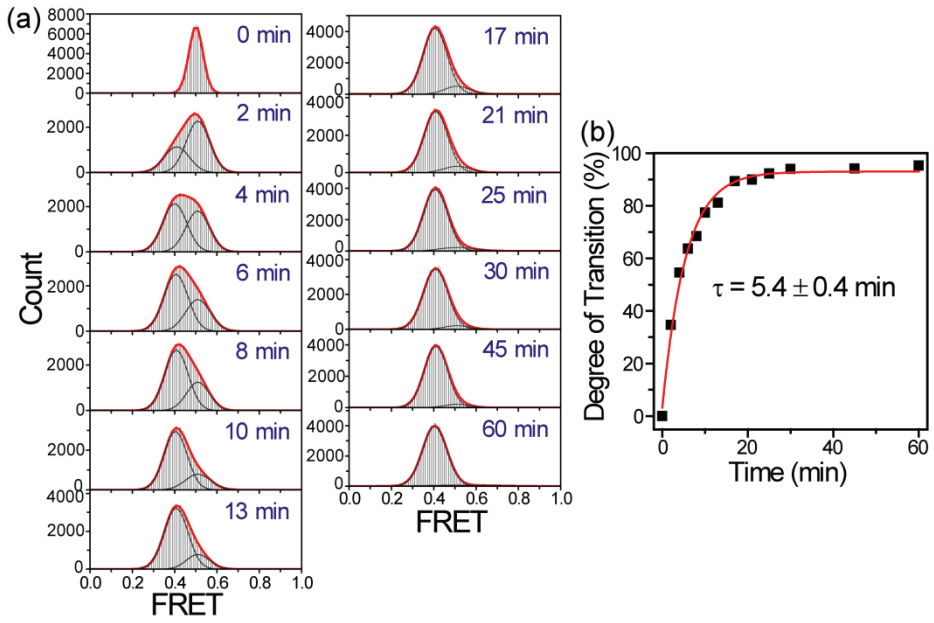

Figure 4.4. Protein-induced B-to-Z transition time. (a) Time-lapse FRET histograms after a rapid delivery of 50 μM hZα$_{ADAR1}$. The experiments were performed at 25 °C. Data acquisition was done for a minute starting 30 s before the designated time. Each histogram was made from more than 400 molecules. (b) By fitting the population to two Gaussian functions, we obtained the delay time of the B-to-Z transition, 5.4 min.

4.3.2. B-to-Z transition rates in the presence of ZBPs are identical to the intrinsic B-to-Z transition rates

To answer whether $hZ\alpha_{ADAR1}$ is playing an active role or a passive role in this B-to-Z transition, it is important to compare the intrinsic B-to-Z transition rate with the transition rate in the presence of $hZ\alpha_{ADAR1}$. Since $hZ\alpha_{ADAR1}$ did not work under high salt conditions, we needed to find a low salt condition where intrinsic Z-DNA is formed. To increase the probability of Z-DNA formation under low salt conditions, we prepared another DNA duplex containing 5-methyl dCs in the CG-repeat [28] and tested various multivalent ions for ability to induce Z-DNA at low salt concentrations. When millimolar Ni2+ ions were added, DNA duplexes started to repeatedly switch between B-form (the high FRET state) and Z-form (the low FRET state) [Fig. 4.5(a)] whereas such a FRET transition was not observed with other multivalent ions (Fig. 4.6) [29]. This is the first time that B-Z transitions are observed for relaxed DNA, allowing us to determine the intrinsic B-Z transition rates by analyzing dwell-times in B-form and Z-form. With escalating Ni^{2+} concentration, Z-DNA dwell-time linearly increased whereas B-DNA dwell-time monotonically decreased [Fig. 4.5(b)].

After determining intrinsic B-Z transition rates at various Ni^{2+} concentrations, we investigated the effect of $hZ\alpha_{ADAR1}$ binding on the B-to-Z transition rates by rapidly delivering both $hZ\alpha_{ADAR1}$ (50 μM) and Ni^{2+} into the detection chamber. Similarly to the unmethylated DNA substrate, fluorescence intensities were instantaneously increased with the protein

injection, indicating rapid binding of $hZ\alpha_{ADAR1}$ while actual B-to-Z transitions occurred with time delays after the protein binding [Fig. 4.5(c)]. Comparison of this time delays with the intrinsic B-to-Z transition times showed remarkable similarity in the whole range of Ni^{2+} concentrations tested [Fig. 4.5(d)], clearly demonstrating that $hZ\alpha_{ADAR1}$ does not accelerate Z-DNA formation. We obtained the same result with a different Z-DNA forming sequence (Fig. 4.7). Thus, this conclusion seems to be general although further systematic studies with different DNA sequence and other ZBPs would be needed to make the result more conclusive. In the absence of Ni^{2+} ions, we could not directly observe intrinsic B-Z transitions, but the protein-assisted B-to-Z transition was still efficient. Combination of two observations—the conformational selection mechanism of ZBPs in B-to-Z transition and efficient conversion of relaxed B-DNA into Z-DNA at low salt conditions by ZBPs—strongly suggests that intrinsic B-Z transition dynamics really exist in the relaxed state of DNA at physiological salt concentrations, and thereby ZBPs efficiently trap even undetectably low presence of transient Z-DNAs.

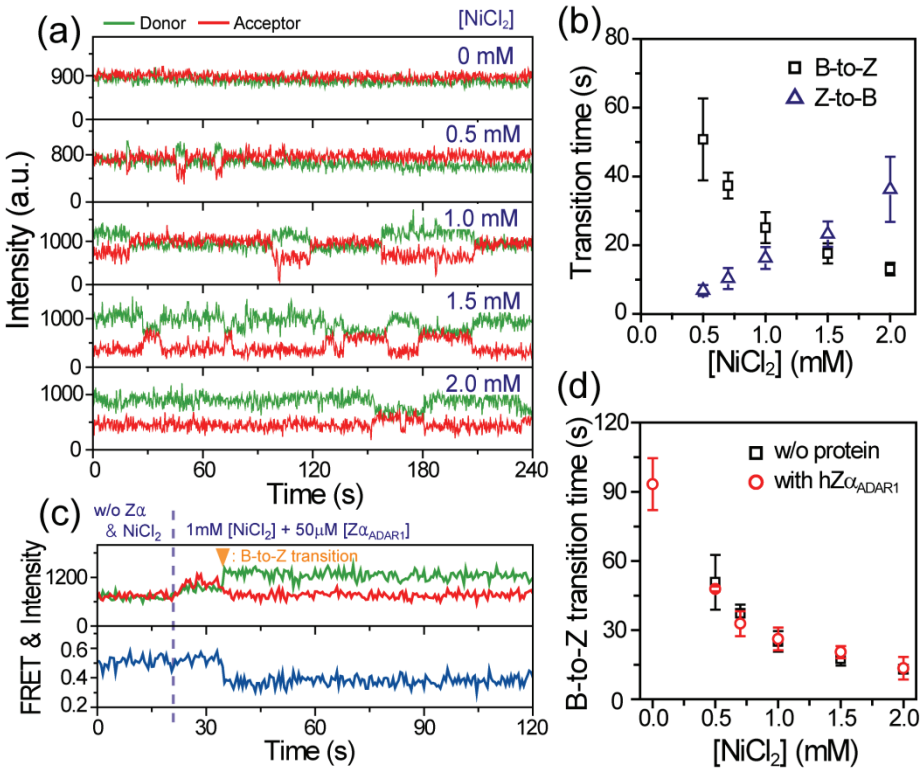

Figure 4.5. Passive trapping, rather than active inducing. (a) Intrinsic BZ transition dynamics of cytosine-methylated DNA duplexes. Typical fluorescence intensity time traces of donor (green lines) and acceptor (red lines) at various Ni^{2+} concentrations are shown. (b) Dwell-times of B-form (black upper triangles) and Z-form (blue lower triangles) at various Ni^{2+} concentrations. (c) Representative fluorescence intensity time traces of donor (green lines) and acceptor (red lines) of $hZ\alpha_{ADAR1}$ delivery experiments (d) Comparison of B-to-Z transition times in the presence of $hZ\alpha_{ADAR1}$ (red circles), and in the absence of $hZ\alpha_{ADAR1}$ (black squares) at various Ni^{2+} concentrations. All experiments were performed at 37 ^{o}C

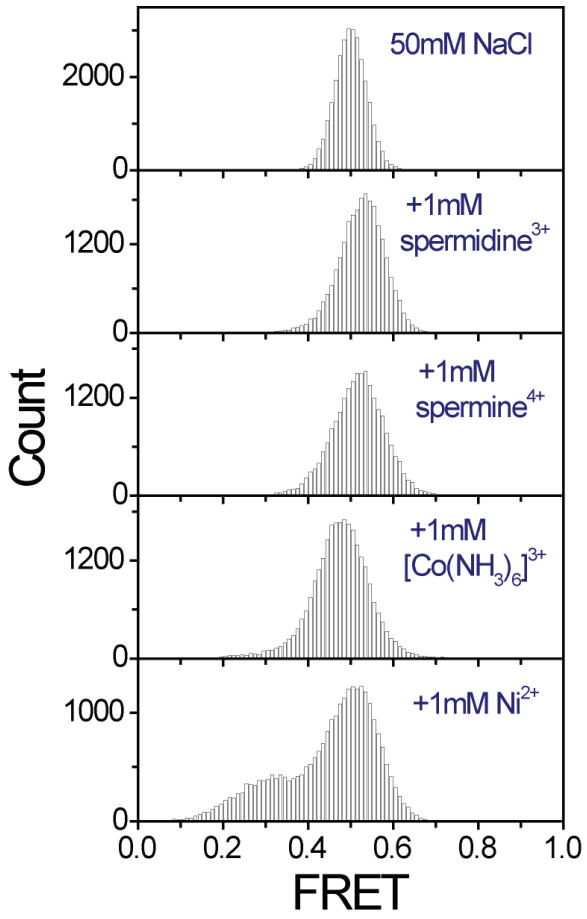

Figure 4.6. FRET histograms of methylated $B(CG)_6$ sample under various salt conditions [7,8]. The experiments were performed at 25 ^{o}C.

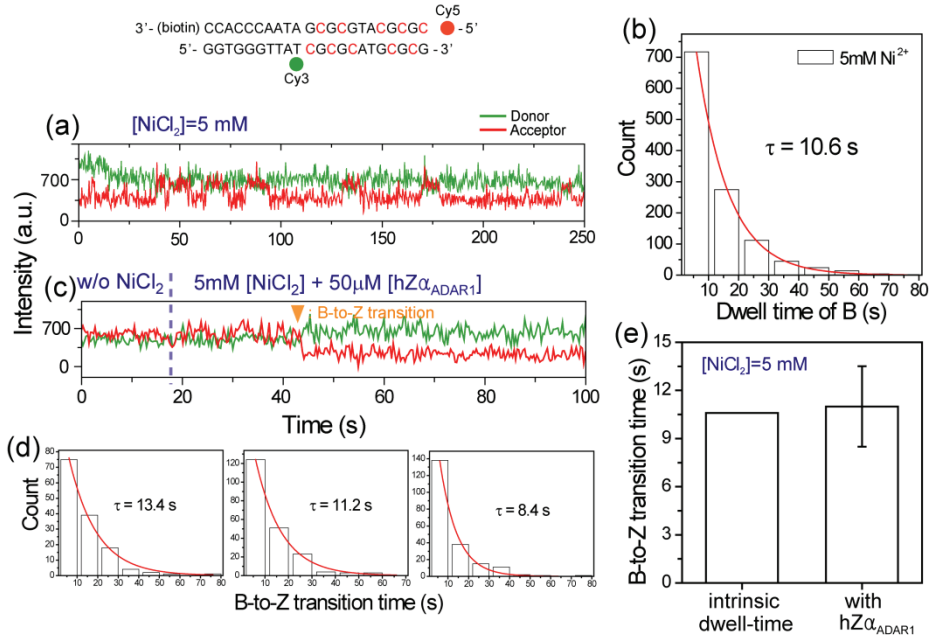

Figure 4.7. (a) Intrinsic BZ transition dynamics of another cytosine-methylated DNA duplexe (DNA sequences are shown at the top) was observed in the presence of 5 mM Ni^{2+}. (b) A dwell-time histogram of B-DNA was made from the experiments described in (a). (c) Representative fluorescence intensity time traces of donor (green lines) and acceptor (red lines) of $hZ\alpha_{ADAR1}$ delivery experiments. (d) B-to-Z transition delay time histograms after the rapid delivery of $hZ\alpha_{ADAR1}$ and Ni^{2+} ions. By fitting the histograms to single-exponential functions, we obtained the B-to-Z transition times. The experiments were repeated three times to obtain the error bar in (e). Comparison of B-to-Z transition times in the presence of (right), and in the absence of $hZ\alpha_{ADAR1}$ (left) at 5 mM Ni^{2+} concentration. The experiments were performed at 37 ^{o}C.

The fact that ZBPs play a passive role in B-to-Z transition suggests that ZBPs may have a strong binding affinity to preformed Z-DNAs. To study the conformational specificity of ZBPs in the dissociation step, we compared dissociation times of ZBPs from B-DNA and Z-DNA. To measure the dissociation time of $hZ\alpha_{ADAR1}$ from Z-DNA, we initially converted all DNAs into Z-form by incubating the unmethylated DNA duplexes for an hour with 50 μM $hZ\alpha_{ADAR1}$ and then removed free $hZ\alpha_{ADAR1}$ from the detection channel. The protein dissociation times were calculated from the time-lapse FRET histograms (Fig. 4.8). To measure the protein dissociation times from B-form DNA, we incubated the DNA duplexes with 50 μM of $hZ\alpha_{ADAR1}$ for 5 minutes, a long enough time for establishing a binding equilibrium but short enough for appreciable amount of DNAs still remaining as B-form. And free proteins then rapidly removed from the detection chamber by changing buffer. Protein dissociation could be monitored by the stepwise decrease of fluorescence intensity of the acceptor (Fig. 4.9). As summarized in Fig. 4.10(a), a dramatic discrimination between B- and Z-DNA was observed in the dissociation step (only 4.4 s for B-DNA, but many hours for Z-DNA), reflecting the "conformational selection" mechanism.

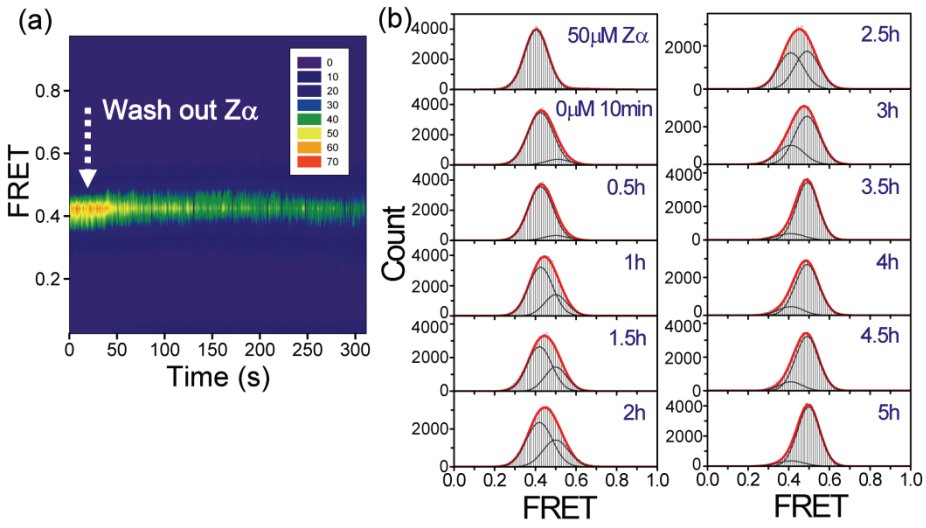

Figure 4.8. Dissociation of $hZ\alpha_{ADAR1}$ from Z-DNA. (a) Time-resolved population FRET histogram of buffer exchange experiment. After incubating the sample for an hour with 50 μM $hZ\alpha_{ADAR1}$, free $hZ\alpha_{ADAR1}$ was washed out at 20 s (white dashed arrow). The experiment was performed in a standard buffer at 25 ^{o}C. No change of FRET population was observed for initial 5 minutes. (b) FRET histograms at various delay times after the washing-out. Data acquisition was done for a minute starting 30 s before the designated time. The population was made from more than 400 molecules. By fitting the population to two Gaussian functions, we obtained the portion of Z-DNA populations [black squares in Fig. 4.10.(a)].

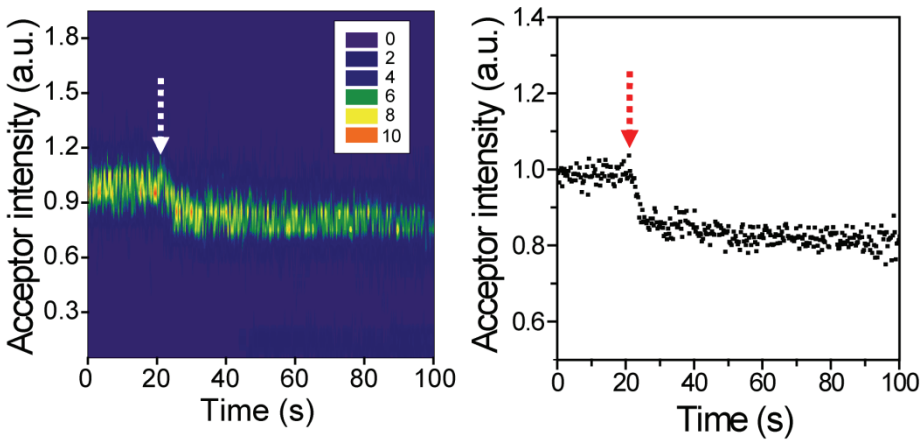

Figure 4.9. Dissociation of $hZ\alpha_{ADAR1}$ from B-DNA. Time-resolved population histogram of Cy5 fluorescence intensity (on the left). After incubating the sample for 5 minutes with 50 μM $hZ\alpha_{ADAR1}$, free $hZ\alpha_{ADAR1}$ was washed out at 23 s (white dashed arrow). The experiment was performed 25 ^{o}C. Data analysis was done only with the molecules whose FRET value did not change during the incubation time. The average intensity of Cy5 fluorescence before the washing-out event was normalized to 1. When $hZ\alpha_{ADAR1}$ proteins dissociate from B-DNA, stepwise decrease of Cy5 fluorescence was observed (left box).Average fluorescence intensity as a function of time from time-resolved population histogram is shown in the right. The transition region was fitted to a single exponential function to get the dissociation time, 4.0 ± 0.4 s.

4.3.3. Z-DNAs are stabilized by selective trapping of transient Z-DNAs by ZBPs

To understand the origin of Z-DNA specificity of ZBPs more deeply, we performed a study of a mutant $hZ\alpha_{ADAR1}$ protein. The previous X-ray crystal structure of a Z-DNA complexed with $hZ\alpha_{ADAR1}$ proteins showed that the tyrosine residue at the 177th position forms CH-π interaction directly with the guanine base in the Z-form of the CG repeats [31]. To investigate the importance of the hydroxyl group of the Tyr-177 in Z-DNA specificity, we performed buffer exchange experiments with a mutant where the tyrosine is replaced with a phenylalanine, $hZ\alpha_{Y177F}$, in the same way as in Figure 3a. Consistently with the expectation, the dissociation time of $hZ\alpha_{Y177F}$ from Z-DNA was greatly reduced [Fig. 4.10(b) and Fig. 4.11], confirming that the interaction between the tyrosine and the guanine base is crucial for the Z-DNA specificity of $hZ\alpha_{ADAR1}$. However, the fact that the Z-DNA stabilizing capability of $hZ\alpha_{Y177F}$ was not completely abolished (Fig. 4.12) indicates that other interactions between $hZ\alpha_{ADAR1}$ residues and Z-DNA backbone are still important for the protein's high specificity to Z-DNA.

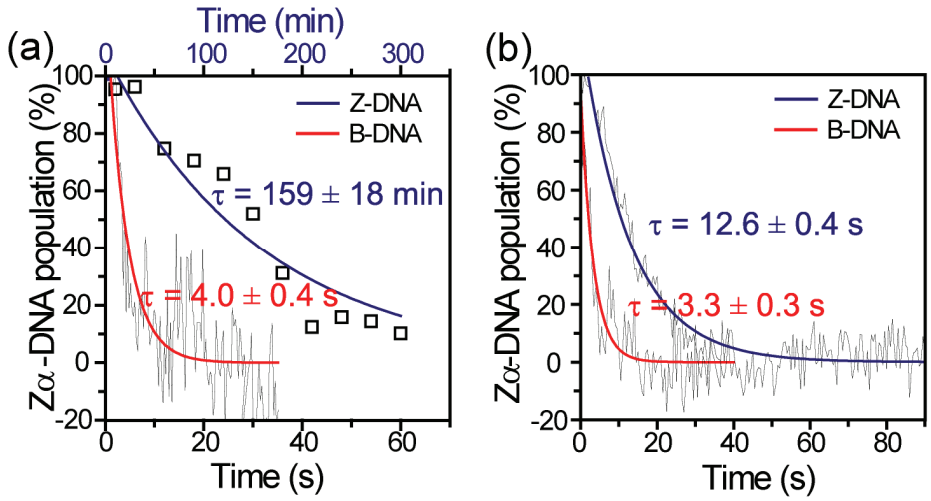

Figure 4.10. Origin of specificity. (a) Dissociation curves of $hZ\alpha_{ADAR1}$ from Z-DNA (blue squares) and from B-DNA (black lines), obtained from rapid buffer exchange experiments in Figure S7, and S8. The dissociation times were obtained by fitting the data to single-exponential curves (blue for Z-DNA, and red for B-DNA). (b) Dissociation curves of $hZ\alpha_{Y177F}$ from Z-DNA and B-DNA (black lines), obtained from rapid buffer exchange experiments in Figure S9. The dissociation times were obtained by fitting the data to single-exponential curves (blue for Z-DNA, and red for B-DNA). All experiments were performed at 25 ^{o}C.

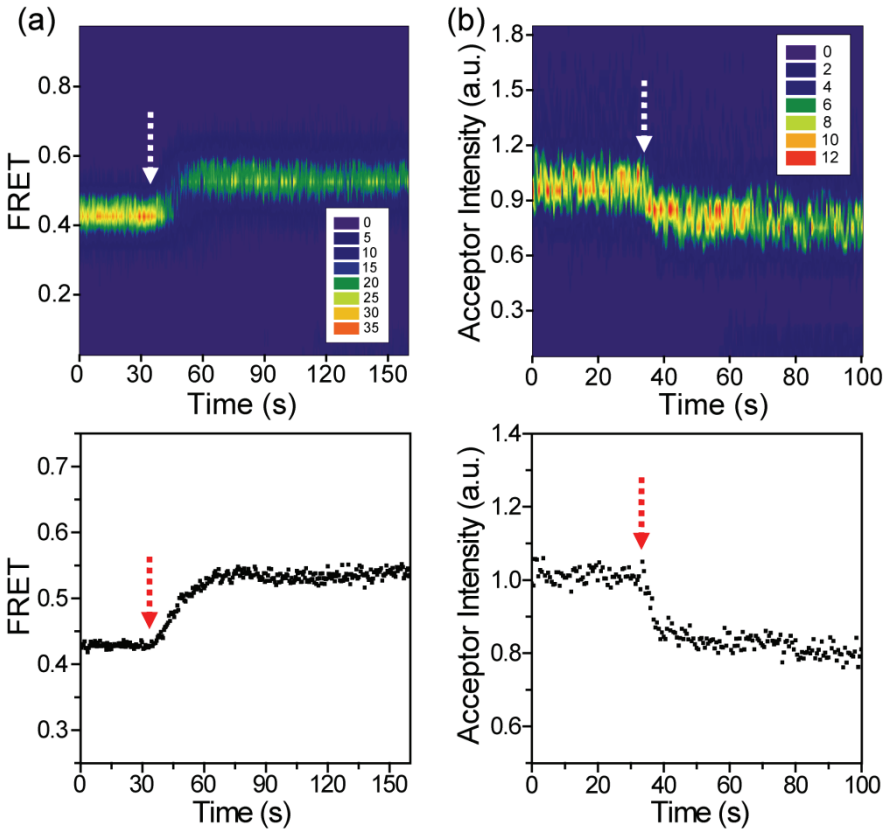

Figure 4.11. Dissociation of hZα$_{Y177F}$ from Z-DNA and B-DNA. (a) Dissociation of hZα$_{Y177F}$ from Z-DNA. Time-resolved population FRET histogram (top). After incubating the sample for an hour with 50 μM hZα$_{Y177F}$, free hZα$_{Y177F}$ was washed out at 34 s (white dashed arrow). The experiment was performed at 25 ^{o}C. FRET as a function of time was obtained by average the FRET histogram in the top graph (bottom). By fitting the transition region, we obtained the Z-to-B transition time as 12.6 ± 0.5 s. (b) Dissociation of hZα$_{Y177F}$ from B-DNA. Time-resolved population histogram of Cy5 fluorescence intensity (top). After incubating the sample for 10 minutes in a standard buffer with 50 μM hZα$_{Y177F}$, free hZα$_{Y177F}$ was washed out at 34 s

(white dashed arrow). The experiment was performed 25 ^{o}C. Data analysis was done only for the molecules whose FRET value did not change during the incubation time. The average intensity of Cy5 fluorescence before the washing-out event was normalized to 1. When h$Z\alpha_{Y177F}$ proteins dissociate from B-DNA, stepwise decrease of Cy5 fluorescence was observed. Average fluorescence intensity as a function of time was obtained from the top graph (bottom). The transition region was fitted to a single exponential function to get the dissociation time of 3.3 ± 0.3 s.

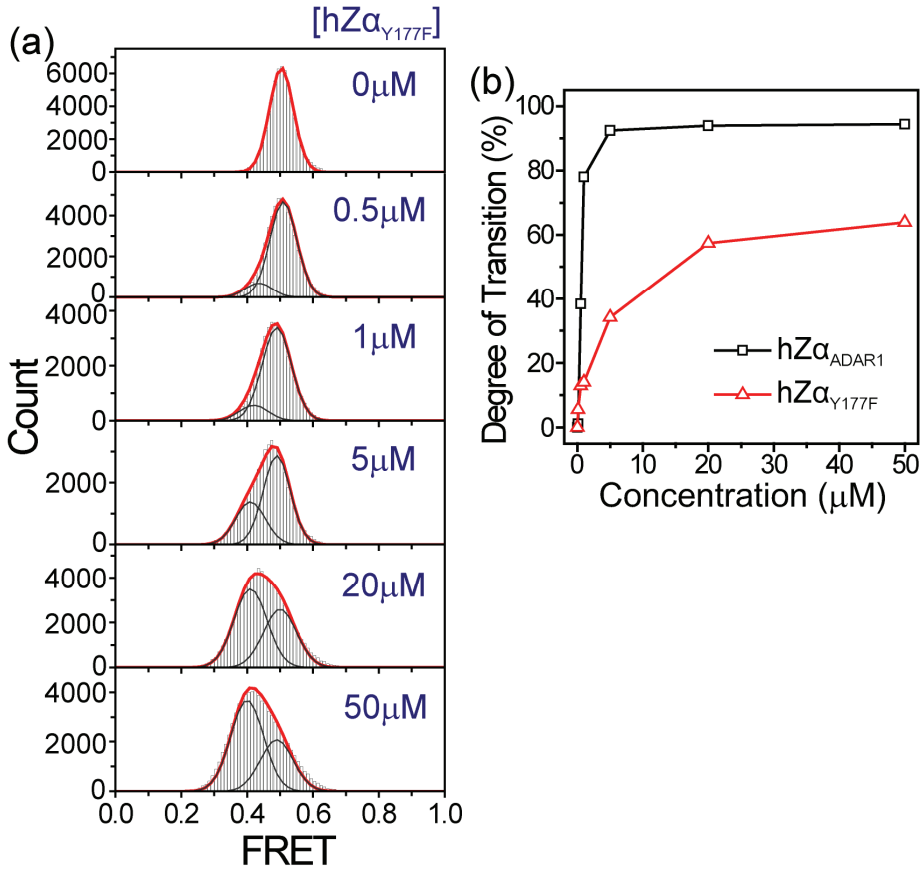

Figure 4.12. B-to-Z transition induced by hZα$_{ADAR1}$ and hZα$_{Y177F}$. (a) FRET histograms of a DNA duplex with at various hZα$_{Y177F}$ concentrations at 25 ^{o}C. The DNA sequence and labeling scheme are same as Fig. 4.1(a). (b) By fitting the population to two Gaussian functions, we obtained the degree of BZ transition (red triangle). Fraction of Z-DNA is somewhat lower in comparison with hZα$_{ADAR1}$ (black square).

In summary, we demonstrated that ZBPs stabilize Z-DNAs via "conformational selection" mechanism, rather than via "induced fit" mechanism. The conformational selection mechanism of ZBPs evidenced in this work may have an implication for the study of other DNA-deformation-inducing proteins [32]: the dynamic nature of DNA structure has a critical role in the genome-wide search for the recognition sites by proteins. Such recognition process is initiated by thermally induced spontaneous fluctuations of DNA structures, not by active participation of proteins.

4.4. References

[1] E. Fisher, *Dtsch. Chem. Ges.* **1894**, 27, 2984-2993.

[2] S. Klimasauskas, S. Kumar, R. J. Roberts, X. Cheng, *Cell* **1994**, 76, 357-369.

[3] Y. Kim, J. H. Geiger, S. Hahn, P. B. Sigler, *Nature* **1993**, 365, 512-520.

[4] F. K. Winkler, D. W. Banner, C. Oefner, D. Tsernoglou, R. S. Brown, S. P. Heathman, R. K. Bryan, P. D. Martin, K. Petratos, K. S. Wilson, *EMBO J.* **1993**, 12, 1781-1795.

[5] D. E. Koshland, *Proc. Natl. Acad. Sci. USA* **1958**, 44, 98-104.

[6] H. R. Bosshard, *News Physiol. Sci.* **2001**, 16, 171-173.

[7] J. M. Bui, J. A. McCammon, *Proc. Natl. Acad. Sci. USA* **2006**, 103, 15451-15456.

[8] K. Arora, C. L. Brooks III, *Proc. Natl. Acad. Sci. USA* **2007**, 104, 18496-18501.

[9] K. Okazaki, S. Takada, *Proc. Natl. Acad. Sci. USA* **2008**, 105, 11182-11187.

[10] S. M. Sullivan, T. Holyoak, *Proc. Natl. Acad. Sci. USA* **2008**, 105, 13829-13834.

[11] G. G. Hammes, Y.-C. Chang, T. G. Oas, *Proc. Natl. Acad. Sci. USA* **2009**, 106, 13737-13741.

[12] T. Wlodarski, B. Zagrovic, *Proc. Natl. Acad. Sci. USA* **2009**, 106, 19346-19351.

[13] J. D. Watson, F. H. C. Crick, *Nature* **1953**, 171, 737-738.

[14] A. H.-J. Wang, G. J. Quigley, F. J. Kolpak, J. L. Crawford, J. H. van Boom, G. van der Marel, A. Rich, *Nature* **1979**, 282, 680-686.

[15] A. Rich, S. Zhang, *Nat. Rev. Genet.* **2003**, 4, 566-572.

[16] F. M. Pohl, J. M. Jovin, *J. Mol. Biol.* **1972**, 67, 375-396.

[17] C. K. Singleton, J. Klysik, S. M. Stirdivant, R. D. Wells, *Nature* **1982**, 299, 312-316.

[18] A. Herbert, K. Lowenhaupt, J. Spitzner, A. Rich, *Proc. Natl. Acad. Sci. USA* **1995**, 92, 7550-7554.

[19] T. Schwartz, J. Behlke, K. Lowenhaupt, U. Heinemann, A. Rich, *Nat. Struct. Biol.* **2001**, 8, 761-765.

[20] S. Rothenburg, N. Deigendesch, K. Dittmar, F. Koch-Nolte, F. Haag, K. Lowenhaupt, A. Rich, *Proc. Natl. Acad. Sci. USA* **2005**, 102, 1602-1607.

[21] S. C. Ha, D. Kim, H.-Y. Hwang, A. Rich, Y.-G. Kim, K. K. Kim, *Proc. Natl. Acad. Sci. USA* **2008**, 105, 20671-20676.

[22] Y.-M. Kang, J. Bang, E.-H. Lee, H.-C. Ahn, Y.-J. Seo, K. K. Kim, Y.-G. Kim, B.-S. Choi, J.-H. Lee, *J. Am. Chem. Soc.* **2009**, 131, 11485-11491.

[23] T. Ha, Th. Enderle, D. F. Ogletree, D. S. Chemla, P. R. Selvin, S. Weiss, *Proc. Natl. Acad. Sci. USA* **1996**, 93, 6264-6268.

[24] R. Roy, S. Hohng, T. Ha, *Nat. Methods* **2008**, 5, 507-516.

[25] M. Lee, S. H. Kim, S.-C. Hong, *Proc. Natl. Acad. Sci. USA* **2010**, 107, 4985-4990.

[26] S. C. Ha, K. Lowenhaupt, A. Rich, Y.-G. Kim, K. K. Kim, *Nature* **2005**, 437, 1183-1186.

[27] S. Myong, S. Cui, P. V. Cornish, A. Kirchhofer, M. U. Gack, J. U. Jung, K.-P. Hopfner, T. Ha, *Science* **2009**, 323, 1070-1074.

[28] M. Behe, S. Zimmerman, G. Felsenfeld, *Nature* **1981**, 293, 233-235.

[29] S. Adam, P. Bourtayre, J. Liquier, E. Taillandier, *Nucl. Acids Res.* **1986**, 14, 3501-3513.

[30] S. C. Ha, N. K. Lokanath, D. Van Quyen, C. A. Wu, K. Lowenhaupt, A. Rich, Y. –G. Kim, K. K. Kim, *Proc. Natl. Acad. Sci. USA* **2004**, 101, 14367–14372.

[31] T. Schwartz, M. A. Rould, K. Lowenhaupt, A. Herbert, A. Rich, *Science* **1999**, 284, 1841-1845.

[30] J. B. Paker, M. A. Bianchet, D. J. Krosky, J. I. Friedman, L. M. Amzel, J. T. Stivers, *Nature* **2007**, 449, 433-437.

Chapter 5. Energetics of different duplexes- DNA, RNA, and hybrid

5.1. Intruction

Z-DNA is a left-handed isoform of Watson-Crick's right-handed B-DNA [1]. The existence of left-handed Z-DNA was first suggested in the circular dischroism measurements performed in high salt conditions [2]. The suspicion of handedness reversal between B-form and Z-form was subsequently confirmed via Raman spectroscopy, and X-ray crystallography [3,4]. Especially, the atomic structure of Z-DNA [5] revealed that contrasted to the case of B-form, in which all bases were in anti-conformation, bases in Z-form alternate between syn- and anti-conformations, providing a natural explanation for why Z-DNA was preferentially formed in purine/pyrimidine repeats [6-8]; syn-conformation was more easily formed in purines than in pyrimidines. Since purine-pyrimidine repeats are abundant in eukaryotic genomes (once every 3000 base pairs in human genome) [9], and non-randomly located in transcription initiation sites [10], it has been speculated that Z-DNA plays a significant role in the regulation of gene transcription [11,12].

Z-DNA is stabilized in vitro by various factors such as methylation, bromination, and multivalent cations [8,13,14]. In cells, Z-DNA is stabilized by negative supercoiling [15,16] and thus Z-DNA formation is critical for

regulating the transcription efficiency and chromatic remodeling [17-20]. Discovery of Z-DNA specific proteins [11,21], called Z-DNA binding proteins (ZBPs), increases the biological significance of Z-DNA. However, characterized biological functions of ZBPs are not directly related to transcription, but diverse: adenosine deaminase acting on RNA (ADAR1), a RNA-editing deaminase; DNA-dependent activator of IFN-regulatory factors (DAI), a cytosolic activator of the innate immune system; E3L, a virulence factor of the poxvirus family involved in the viral pathogenesis, etc. [21-25]. While DAI plays a role in triggering the interferon signal by sensing a cytosolic dsDNA, ADAR1 and E3L negatively regulate the interferon signal by competing with DAI [26]. Furthermore, it was discovered that ZBPs could also stabilize Z-form in RNA [27]. These results suggest that not only their roles in cellular responses but also their natural substrates in cells may be diverse. However, underlying mechanism of Z-form stabilization by ZBPs is still unclear although some significant progresses in our understanding of this interaction are proposed based on various biophysical experiments [28-30].

Here we compared Z-DNA stabilization efficiencies of ZBP in DNA, RNA, and DNA-RNA hybrid duplexes by accurately quantitating Z-form population on each substrate via single-molecule FRET [31]. Unexpectedly, we found that Z-form was most efficiently stabilized by ZBP in the DNA-RNA hybrid, which had a greatly reduced transition barrier of the junction between Z-form and non- Z-form.

5.2. Materials and Methods

5.2.1. Protein, DNA, RNA, and Hybrid sample preparation

Proteins were prepared as described [28]. DNA strands were purchased from Integrated DNA Technologies (Coralville, IA), and labelled with Cy3 or Cy5 as described [32]. DNA duplexes were formed by mixing the biotinylated and non-biotinylated stand in 1:2 ratio at 50 μM concentration in a buffer containing 10mM Tris (pH 8.0) and 50mM NaCl. The non-biotinylated strand was added in excess to minimize the chance of having un-annealed biotinylated strand in the measurement. The annealing mixture was heated at 95 ^{o}C for 3 minutes and allowed to cool down slowly to room temperature for 1.5 hours in a heating block. The RNA strands for R6 were purchased from ST Pharm Co. (South Korea), and labelled with Cy3 or Cy5. The RNA strands for R8 were purchased from Dharmacon Inc. (Lafayette, CO), and labelled with DY547 or DY647. RNA duplexes were prepared by using the same protocol as for DNA except that the annealing buffer contains additional 1m M EDTA.

5.2.2. Experimental methods

Single-molecule FRET measurements. A quartz slide was coated with poly-ethylene glycol (PEG, m-PEG-5000; Laysan Bio Inc.) and 1-2% biotinylated PEG (biotin-PEG-5000; Laysan Bio Inc.) as described [32]. After injecting streptavidin (Sigma, 0.2mg/ml) into channel and immobilizing biotinylated oligonucleotides (100 pM) via a biotin–streptavidin interaction on a polymer-

coated surface, single-molecule fluorescence images were obtained in a wide-field total-internal-reflection fluorescence microscope with 100-ms time resolution using an electron multiplying charge-coupled device (EM-CCD) camera (iXon DV887ECS-BV, Andor Technology) and a homemade C++ program. Measurements were performed in an imaging buffer containing 10mM Tris-HCl (pH 8.0), 50 mM NaCl, and an oxygen scavenger system to slow photobleaching: 2.5mM PCA (Sigma-Aldrich), 50nM PCD (Sigma-Aldrich), 1% (v/v) Trolox (Sigma-Aldrich) [33].

Bulk FRET measurements. Bulk FRET efficiency was measured by using Varian Eclipse fluorescence spectrophotometer. Oligonucleotide duplex (10nM) was incubated in a buffer containing 10 mM Tris-HCl (pH 8.0) and 50 μM $hZ\alpha_{ADAR1}$ at designated temperature. The sample was excited at 500 nm and emission fluorescence signals at 565 nm and 665 nm were measured for Cy3 and Cy5, respectively. FRET efficiency was calculated by $I_{665nm}/(I_{565nm}+I_{665nm})$, where I_{peak} means the fluorescence intensity at the peak wavelength.

5.2.3. Analysis -Determination of thermodynamic parameters

To obtain the entropy and enthalpy of Z-form transition, equilibrium constants (Keq) at varying temperatures (T) were fitted to the van't Hoff equation: $\ln(K_{eq}) = \frac{\Delta S^o}{R} - \frac{1}{T}\frac{\Delta H^o}{R}$, where R, ΔS^o, and ΔH^o are the ideal gas constant, the transition entropy, and the transition enthalpy, respectively. To obtain the

enthalpic barriers of Z-form transition, we first determined the forward transition rate (kf: the transition rate from non-Z-form to Z-form) and the backward transition rate (kb: the transition rate from Z-form to non-Z-form) at each temperature by solving the following equations: $K_{eq} = \frac{k_f}{k_b}$, and $\tau^{-1} = k_f + k_b$, where τ is the kinetic time constant obtained from bulk FRET measurement. Then, temperature-dependent reaction rates (k: kf or kb) were fitted to the Arrhenius equation: $\ln(k) = A - \frac{1}{T}\frac{\Delta H^{\ddagger}}{R}$, where A, and $\Delta H^{\ddagger}$ are a fitting constant, the entropic barrier of the transition, respectively [34].

5.3. Results

5.3.1. Z-form of DNA-RNA hybrid is most efficiently stabilized by ZBP

Z-form of nucleic acids is preferably formed in purine-pyrimidine repeats, rendering a high chance in a biological context that Z-form is embedded in long stretches of non-Z-form such as dsDNA in B-form. With this in mind, we prepared dye-labelled DNA, RNA, and DNA-RNA hybrid duplexes, which had CG-repeats in the center with flanking random sequences (Fig. 5.1). The thymine base at the junction of Z-form and non-Z-form was selected as labelling positions of fluorophores to maximize FRET change during Z-transition [28,30], and one end of the duplexes was biontinylated for surface immobilization. Depending on the duplex composition (D for DNA, R for RNA, and H for hybrid) and the number of the central CG repeat (n), each

sample was named as Dn, Rn, and Hn, respectively. For instance, D6 refers to a DNA duplex with six CG repeats at the center.

First, we measured the kinetics of the Z-form transition after adding the Zα domain of human double stranded RNA adenosine deaminase ($hZ\alpha_{ADAR1}$). Fig. 5.2(a)-(c) show the bulk FRET traces for D6, R6, and H6 after 50 μM of $hZ\alpha_{ADAR1}$ was added at 29 ^{o}C. It is noticeable that the equilibrium is reached significantly faster in H6 than in R6 or D6.

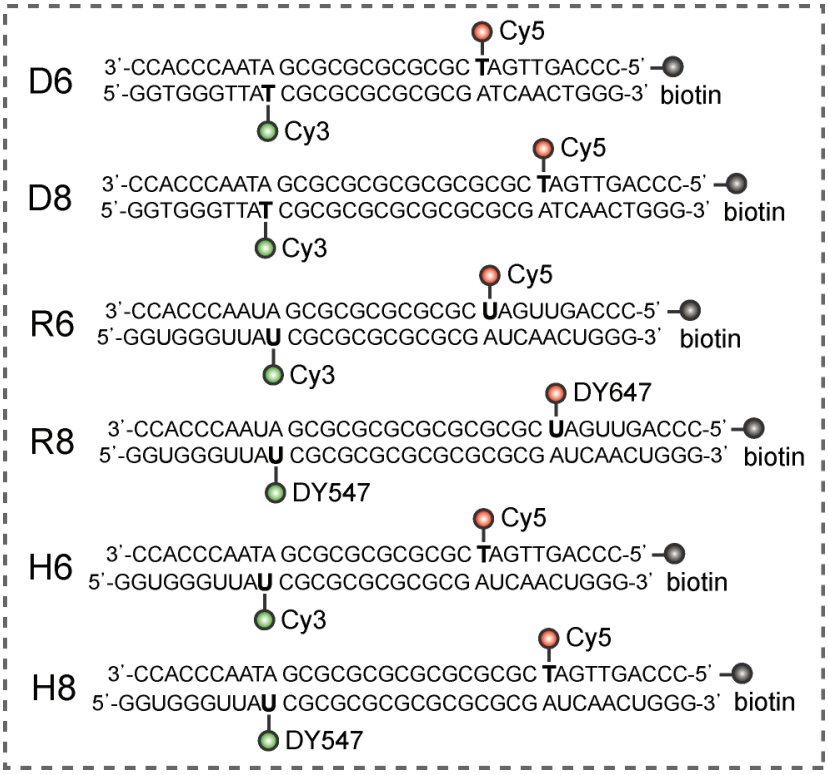

Figure 5.1. Design of DNA, RNA, and DNA-RNA duplexes for the experiments. Oligotide sequences and modification sites are indicated for each sample.

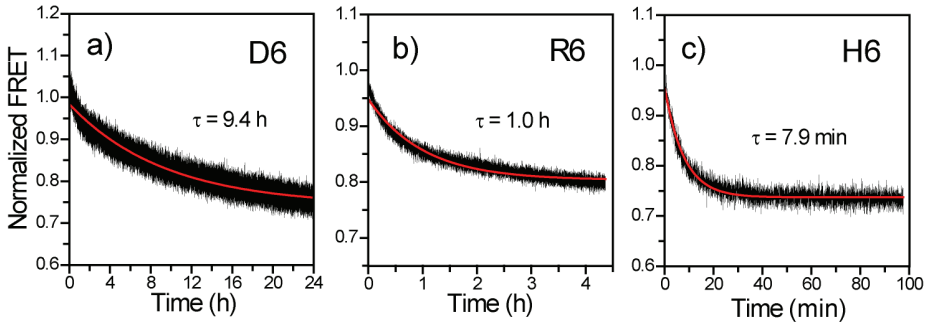

Figure 5.2. Comparison of Z-form transition kinetics by ZBP. Bulk FRET time traces of D6 (a), R5 (b), and H6 (c) after adding 50 μM of $hZ\alpha_{ADAR1}$ are shown. The transition times were obtained by fitting the data to a single exponential function.

Next, we performed single-molecule FRET experiments to quantitate Z-form population at equilibrium. Duplex oligonucleotides were immobilized on a polymer-coated quartz surface via streptavidin-biotin interaction, and incubated with varying concentrations of $hZ\alpha_{ADAR1}$. The incubation time was chosen based on the time constants measured in Fig. 5.2(a)-(c) to ensure that the equilibrium of Z-form transition is established. Single-molecule images were obtained in a wide-field total-internal-reflection fluorescence microscope. Fig. 5.3(a)-(c) show FRET histograms of D6, R6, and H6 incubated with designated $hZ\alpha_{ADAR1}$ concentrations, respectively. As previously reported [30], the low FRET state appearing at high $hZ\alpha_{ADAR1}$ concentrations indicates the presence of Z-DNA. The FRET histograms were well fitted to a sum of two Gaussian functions, providing a way to accurately quantitate the Z-form population at equilibrium. It is clear that Z-form is most efficiently formed in H6. However, we did not see a correlation between the phenominological dissociation constants of $hZ\alpha_{ADAR1}$ (K_d: the $hZ\alpha_{ADAR1}$ concentration at which half of saturated Z-form population is reached) and Z-form stabilization efficiencies [Fig. 5.3(d)]. Besides, there is almost no difference in binding affinities of $hZ\alpha_{ADAR1}$ for DNA, RNA, DNA-RNA hybrid duplexes comprising CG repeats determined by the analytical ultracentrifugation. Therefore, this high efficiency of Z-form stabilization in the DNA-RNA hybrid is not due to the high binding efficiency of $hZ\alpha_{ADAR1}$ to the hybrid duplex.

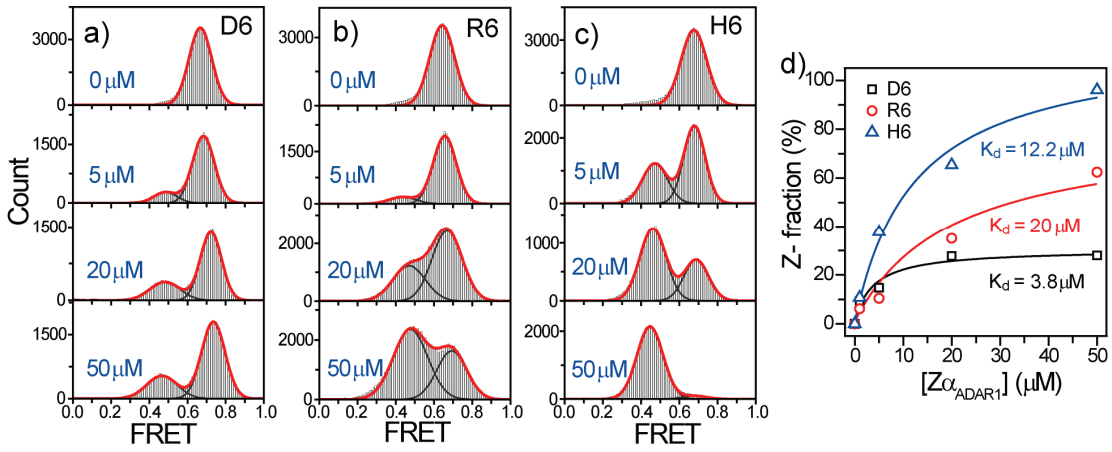

Figure 5.3. Comparison of Z-form stabilization efficiencies of ZBP. Single-molecule FRET histograms of D6 (a), R6 (b), and H6 (c) at varying $hZ\alpha_{ADAR1}$ concentrations are shown. (d) Z-form population as a function of $hZ\alpha_{ADAR1}$ concentration. The phenomenological dissociation constants of $hZ\alpha_{ADAR1}$ (K_d) were obtained by fitting the data to a Hill equation (n = 1). All experiments were performed at 29 ^{o}C.

5.3.2. Z-form is favoured at higher temperatures

To obtain thermodynamic and kinetic understanding of why Z-form is most favoured in the DNA-RNA hybrid duplex, we investigated the temperature dependence of Z-form stabilization in the presence of the saturation amount of $hZ\alpha_{ADAR1}$ (50 μM). Fig. 5.4(a) shows FRET histograms of D6 at five different temperatures. Likewise, Z-form population was measured at various temperatures for D8 (Fig. 5.5), R6 and R8 (Fig. 5.6), and H6 and H8 (Fig. 5.7). These results are summarized in Fig. 5.4(b)-(d), (left).

In all samples, Z-form became more populated with increasing temperature [Fig. 5.4(b)-(d), left], indicating that Z-form stabilization is an endothermic process. Since binding of ZBP is apparently an exothermic process, we infer that the observation indicates that even though the binding energy of ZBPs is utilized for Z-form stabilization, intrinsic conformational dynamics of nucleic acid duplexes still dominates the Z-form transition by ZBPs [30]. Thermodynamic parameters obtained from temperature dependence of Z-form and non-Z-form equilibrium are summarized in Table 5.1. Interestingly, we found that there existed an enthalpy-entropy competition; the enthalpic term hindered Z-form formation while the entropic term helped the transition.

The equilibrium constant of Z-form transition obtained in single-molecule FRET measurements provides a ratio between a forward rate (k_f: the transition rate from non-Z-form to Z-form) and the backward rate (k_b: the transition rate from Z-form to non-Z-form) while the kinetic time constant of Z-form transition obtained in bulk FRET measurements as in Fig. 5.2(a)-(c) provides

the sum of the forward and backward rates. By combining the equilibrium constants [Fig. 5.4(b)-(d), left], and the kinetic time constants (Fig. 5.8-5.10), we determined the forward and backward rate constants for each temperature. Both the forward rate [Fig. 5.4(b)-(d), middle] and the backward rates [Fig. 5.4(b)-(d), right] of Z-form transition increased with temperature, indicating that an enthalpic barrier should be overcome for the transitions in both directions. Thermodynamic parameters obtained from temperature dependence of the transition rates are summarized in Table 5.1. Interestingly, although Z-form transition equilibrium was reached most rapidly in the hybrid sample (H6 and H8), the enthalpic barrier of the hybrid duplexes was higher than those of other two. This observation indicates that the hybrid duplex has the largest pre-exponential factor among the three kinds of duplexes, probably due to its smallest entropic barrier.

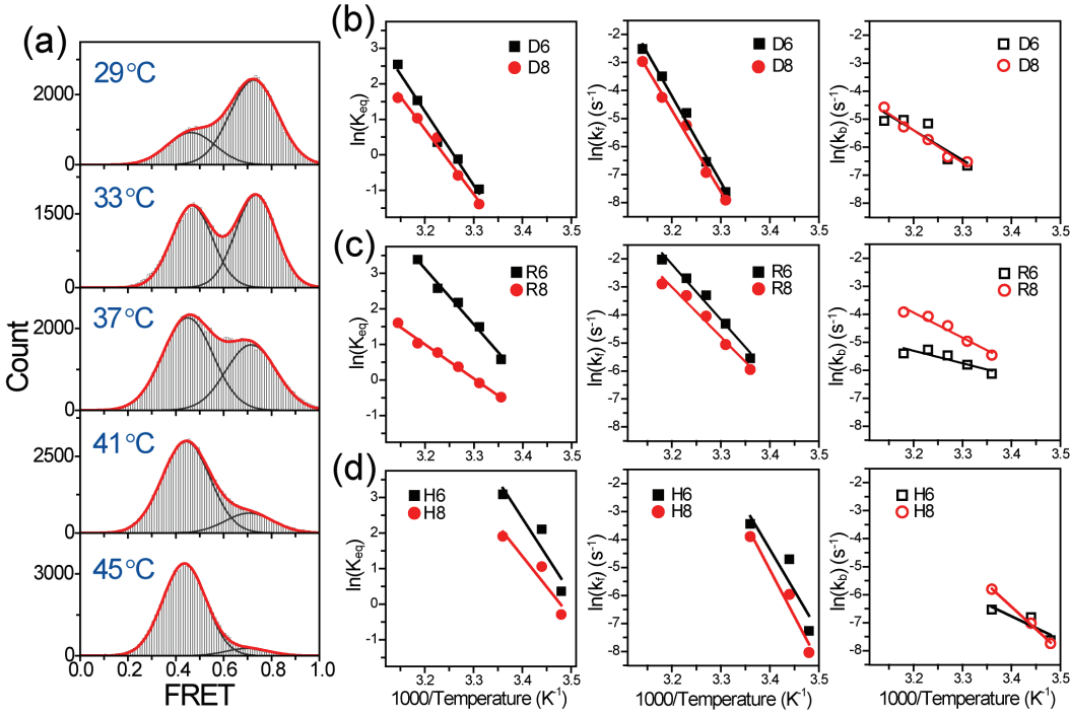

Figure 5.4. Temperature dependence of Z-form formation. (a) FRET histograms of D6 at varying temperatures ([hZα$_{ADAR1}$] = 50 μM). (b) Temperature dependence of Z-form equilibrium constant (left), the transition rate to Z-form (middle), and the transition rate from Z-form (right) for D6 and D8. (c) The same as (b) for R6 and R8. (d) The same as (b) for H6 and H8.

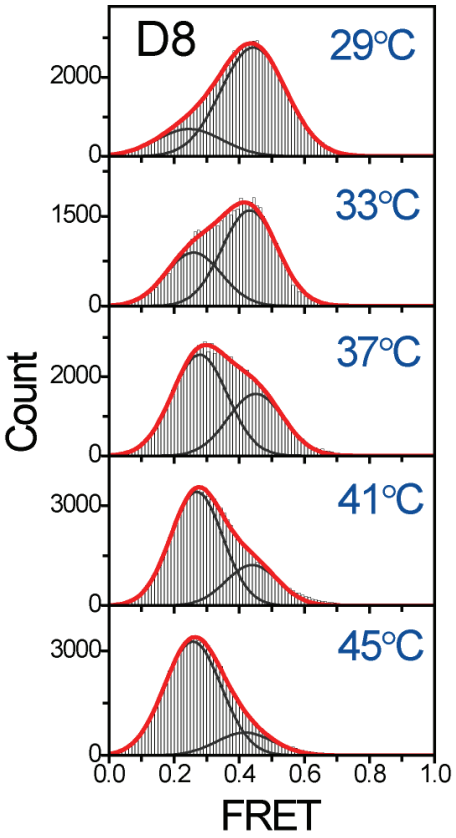

Figure 5.5. FRET histograms of D8 sample with 50 μM of hZα_{ADAR1} at varying temperature. As temperature became higher, Z-form was increased. By fitting two Gaussian functions, non-Z (B-form) and Z-fraction were obtained.

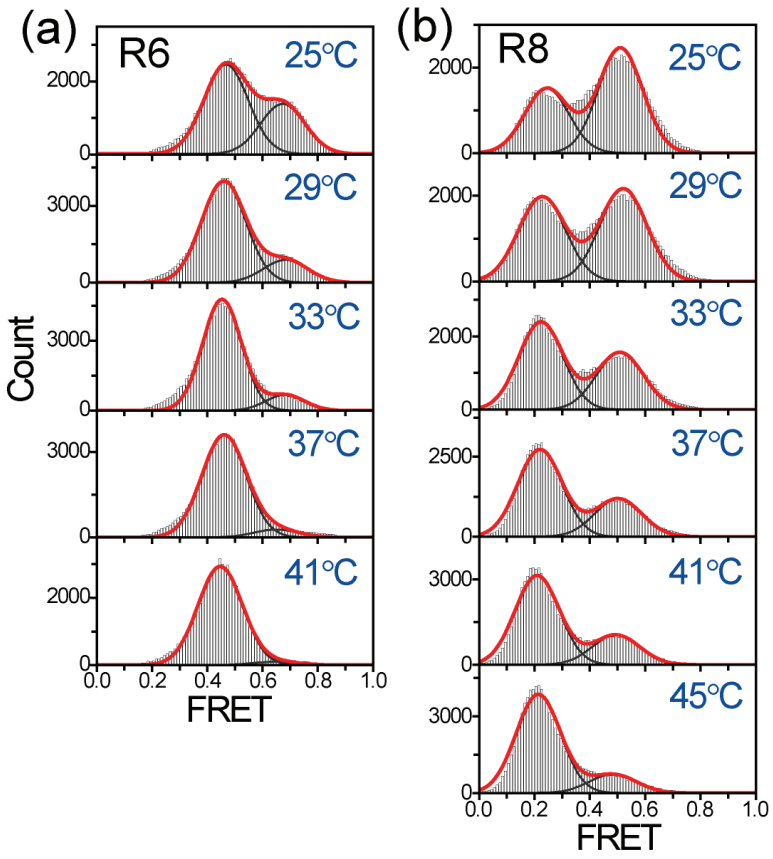

Figure 5.6. FRET histograms of R6 (a) and R8 (b) sample with 50 μM of hZα$_{ADAR1}$ at varying temperature. As temperature became higher, Z-form was increased. By fitting two Gaussian functions, non-Z (A-form) and Z-fraction were obtained.

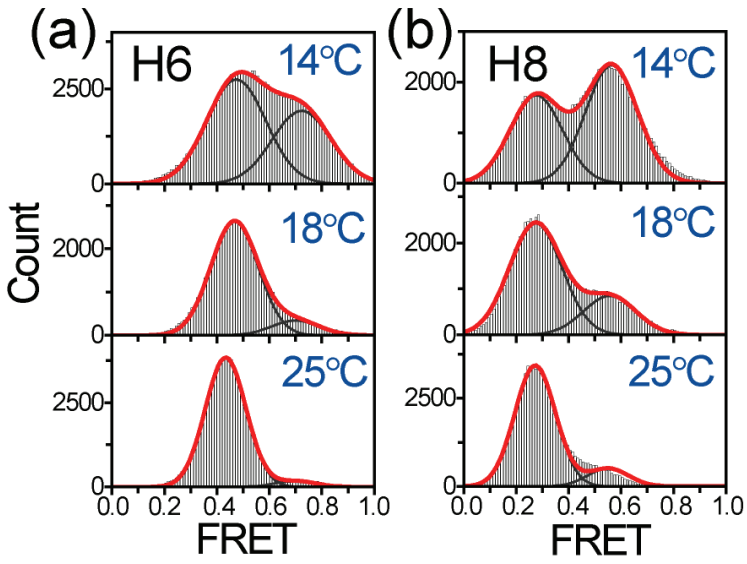

Figure 5.7. FRET histograms of H6 (a) and H8 (b) sample with 50 μM of $hZ\alpha_{ADAR1}$ at varying temperature. As temperature became higher, Z-form was increased. By fitting two Gaussian functions, non-Z (A-form) and Z-fraction were obtained.

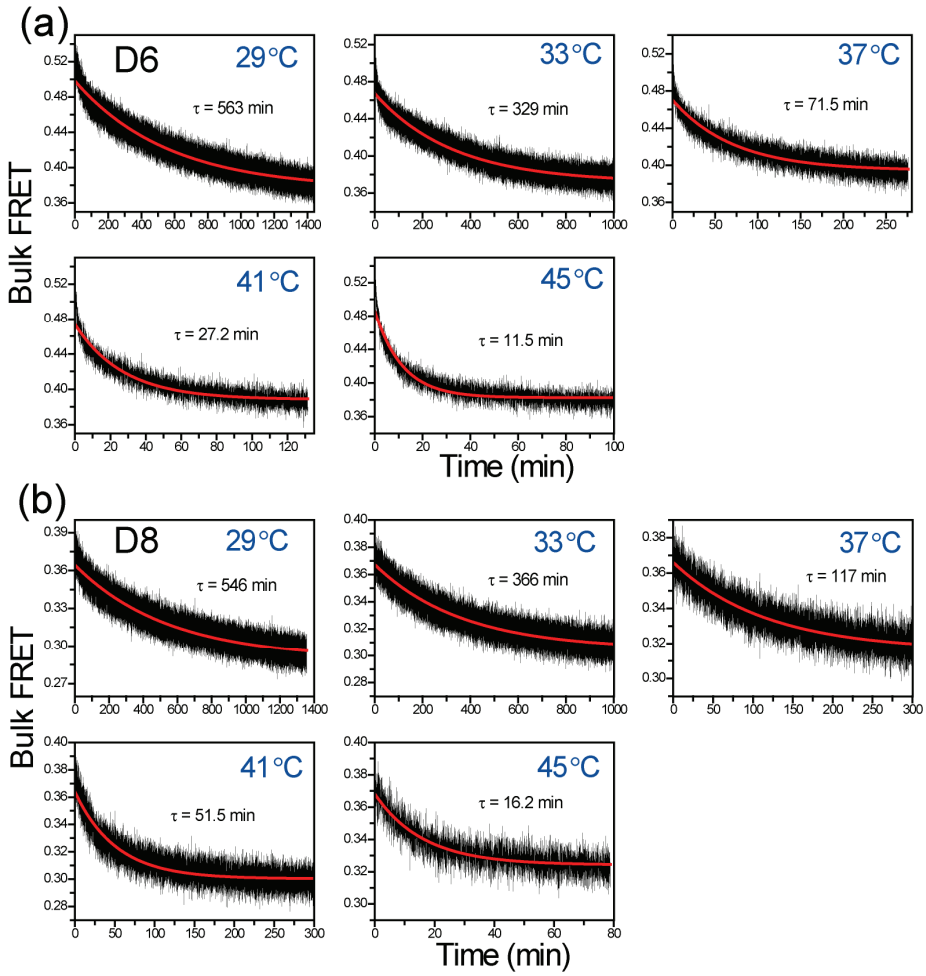

Figure 5.8. Bulk FRET kinetic measurements of D6 (a) and D8 (b) sample on 50 μM of hZα$_{ADAR1}$ concentrations at various temperature. By fitting a single exponential function, half time of transition were obtained..

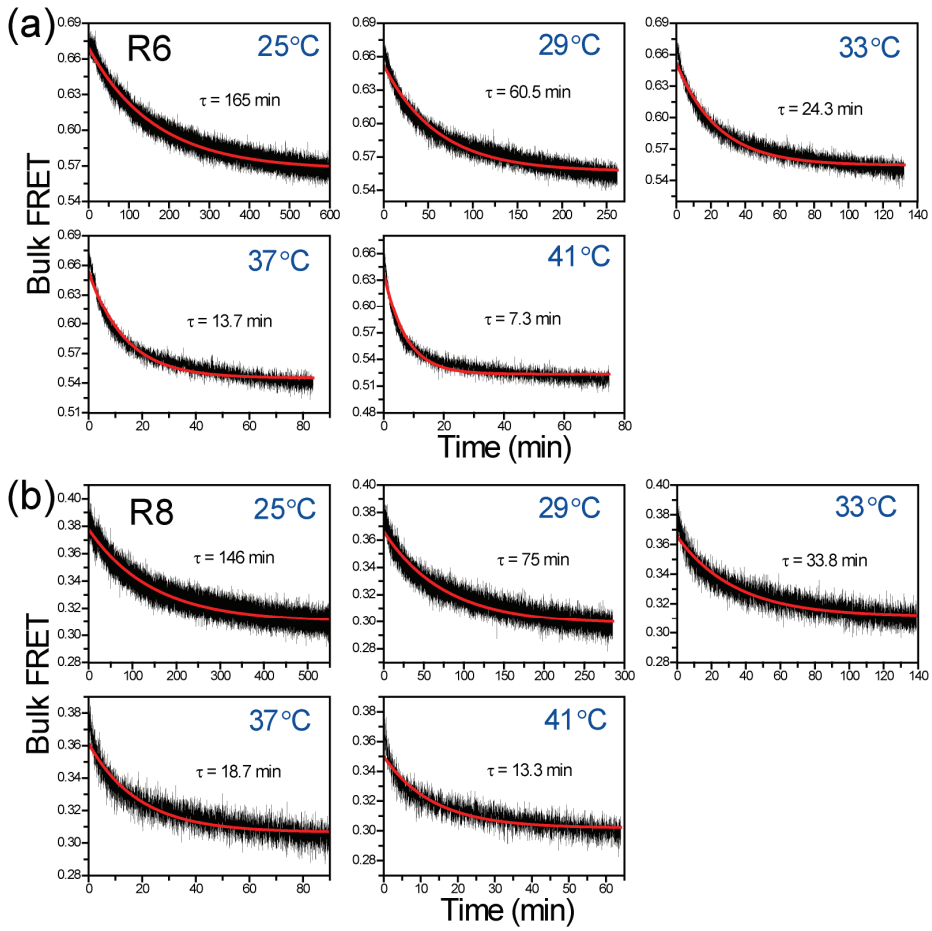

Figure 5.9. Bulk FRET kinetic measurements of R6 (a) and R8 (b) sample on 50 μM of $hZ\alpha_{ADAR1}$ concentrations at various temperature. By fitting a single exponential function, half time of transition were obtained..

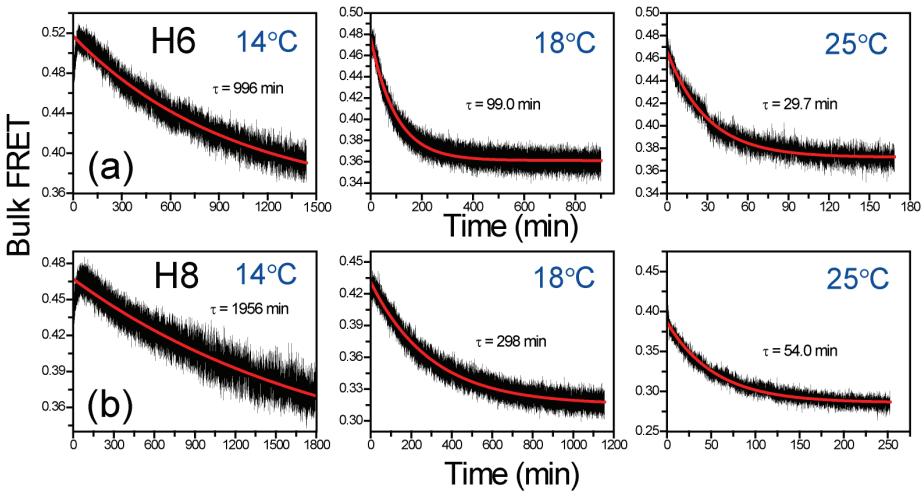

Figure 5.10. Bulk FRET kinetic measurements of H6 (a) and H8 (b) sample on 50 μM of $hZ\alpha_{ADAR1}$ concentrations at various temperature. By fitting a single exponential function, half time of transition were obtained.

Table 5.1. Thermodynamic parameters obtained from Fig. 5.4.

	ΔH° (kcal/mol)	ΔS° (cal/mol/K)	ΔG° (kcal/mol) at 37℃	$\Delta H^{\ddagger}_{f}$ (kcal/mol)	$\Delta H^{\ddagger}_{b}$ (kcal/mol)
D6	41.3±3.5	134.5±11.4	-0.40	61.1±3.5	21.0±6.1
D8	36.3±2.5	117.5±8.1	-0.13	57.9±3.4	23.0±2.2
R6	31.1±2.1	105.8±6.7	-1.70	39.2±3.5	8.9±2.6
R8	19.1±0.8	63.1±2.5	-0.46	35.3±3.4	17.8±2.3
H6	42.2±15.4	148.4±52.8	-3.80	58.7±23.7	16.5±8.3
H8	34.2±11.3	119.1±38.9	-2.72	66.0±12.8	31.8±1.5

The Gibbs free energy (ΔG^{o}) was calculated at 37 ^{o}C.

5.3.2. DNA-RNA hybrid has the lowest junction energy

To further understand the thermodynamic and kinetic basis of the high Z-form formation efficiency and rate in DNA-RNA hybrid duplexes, we decomposed the thermodynamic functions in Table 5.1 into contributions of the junction and the CG repeat (Table 5.2-5.3). Since the contributions of Gibbs free energy of each sample is composed of only two components—the junction and the CG repeat, the thermodynamic functions of the CG repeat and that of the junction could be determined from a pair of samples with the same duplex composition and different CG repeat numbers, eg. H6 and H8. From this analysis, the following conclusions were derived.

Firstly, although the enthalpy-entropy competition is common for both CG repeat and junction, the thermodynamic driving terms to Z-form are distinct for the two contributions: Z-form is enthalpically favoured but entropically disfavoured for the CG repeat while Z-form is entropically driven and requires enthalpic cost for the junction. The result is consistent with the previous observation that the binding interaction of ZBP was mainly observed in the CG repeat [35] and the B-Z junction was disorganized in Z-form [28].

Secondly, preferable junction energy is the cause for the efficient stabilization of the Z-form in the DNA-RNA hybrid duplex: relatively large free energy cost of the CG repeat was compensated by the lowest free energy of the junction for the hybrid sample (Table 5.2). In a similar way, we observed that the largest enthalpic barrier of the CG repeat was compensated by the smallest enthalpic barrier of junction for the hybrid sample (Table 5.3).

In general, the contribution of the junction dominates Z-form transition over the CG repeat contribution for short Z-form stretches, and we infer that structural transitions in the junction are most crucial, kinetically as well as thermodynamically.

Table 5.2. enthalpic and entropic contributions of the CG repeat and the junction to the standard free energy change of Z-form formation.

	DNA			RNA			Hybrid		
	ΔH° (kcal/mol)	ΔS° (cal/mol/K)	ΔG° (kcal/mol) at 37℃	ΔH° (kcal/mol)	ΔS° (cal/mol/K)	ΔG° (kcal/mol) at 37℃	ΔH° (kcal/mol)	ΔS° (cal/mol/K)	ΔG° (kcal/mol) at 37℃
(CG)	-2.5	-8.5	0.1	-6.0	-21.4	0.6	-4.0	-14.7	0.5
Junction	28.2	92.8	-0.6	33.6	117.0	-2.7	33.1	118.2	-3.5

The Gibbs free energy (ΔG^o) was calculated at 37 ^{o}C.

Table 5.3. Contributions of the CG repeat and the junction to the enthalpic barriers.

	DNA		RNA		Hybrid	
	$\Delta H_f^\ddagger$ (kcal/mol)	$\Delta H_b^\ddagger$ (kcal/mol)	$\Delta H_f^\ddagger$ (kcal/mol)	$\Delta H_b^\ddagger$ (kcal/mol)	$\Delta H_f^\ddagger$ (kcal/mol)	$\Delta H_b^\ddagger$ (kcal/mol)
(CG)	-1.6	1.0	-2.0	4.5	3.7	7.7
Junction	35.4	7.5	25.5	-9.0	18.4	-14.7

5.4. Discussions

In discussion, we compared how efficiently and swiftly Z-form was stabilized by ZBP in DNA, RNA, and DNA-RNA hybrid duplexes. Z-form transition was unexpectedly most efficient and rapid in the DNA-RNA hybrid duplex. From the further analysis, the thermodynamic parameters for Z-form transition revealed that the energetic bottleneck of A-to-Z transition in the A-form hybrid duplex was the formation of A-Z junctions in the A-form hybrid duplex. Up to now, in spite of a great deal of information about the in vitro and in vivo activity of ZBPs, and considerable indirect evidence concerning the biological role, the precise substrate for ZBPs has not been determined. Our study revealed that DNA-RNA hybrid was bound with much more favorable kinetics than RNA and DNA duplexex by $hZ\alpha_{ADAR1}$. Thus, it is very intriguing to consider that DNA-RNA hybrid may constitute a biologically relevant ligand for $hZ\alpha_{ADAR1}$ and other ZBPs. In fact, DNA-RNA hybrids occur throughout the cell, both nucleus and cytosol, in many circumstances such as RNA editing and viral pathogenesis: short stretches of Z-forming sequences are prevalent in human and viral genomes [36-39]. During the transcription and viral pathogenesis, numerous potential Z-forming sites are present in DNA-RNA hybrid duplexes. ZBPs present in various proteins may recognize such sequences and promote Z-form formation during the course of finding or reorganizing their target nucleic acid substrates. Thus, it is quite plausible that DNA-RNA hybrids may be one of natural substrates for ZBPs, although the nature of the ligand that they all bind to remains to be

determined—dsDNA, dsRNA or DNA/RNA hybrid.

Our experiment extends the understanding of Z-form transition at the sequences surrounded by right-handed B-form or A-form nucleic acid duplexes. The junction region contributes not only to easing the strain caused by opposite handedness occurring within a duplex, but also promoting swift conformational change toward Z-form. The different sequence context containing CA/TG repeats and even non-purine/pyrimidine repeats other than CG repeats are more frequently present in potential Z-forming sequences in cells. In the future study, thus, our analysis should explore different base pair compositions and lengths of Z-forming sequences for better understanding of Z-from formation in biological processes.

5.5. References

[1] A. Rich, *Gene* **1993**, 135, 99-109.

[2] F. M. Pohl, J. M. Jovin, *J. Mol. Biol.* **1972**, 67, 375-396.

[3] T. J. Thamann, R. C. Lord, A. H. -J. Wang, A. Rick, *Nucl. Acids Res.* **1981**, 9, 5443-5457.

[4] M. Behe, S. Zimmerman, G. Felsenfeld, *Nature* **1981**, 293, 233-235.

[5] A. H.-J. Wang, G. J. Quigley, F. J. Kolpak, J. L. Crawford, J. H. van Boom, G. van der Marel, A. Rich, *Nature* **1979**, 282, 680-686.

[6] J. Kłysik, S. M. Stirdivant, J. E. Larson, P. A. Hart, R. D. Wells, *Nature* **1981**, 290, 672-677.

[7] D. B. Haniford, D. E. Pulleyblank, *Nature* **1983**, 302, 632-634.

[8] A. Rich, A. Nordheim, A. H. -J. Wang, *Ann. Rev. Biochem.* **1984**, 53, 197-846.

[9] H. Hamada, T. Kakunaga, *Nature* **1982**, 298, 396-398.

[10] G. P. Schroth, P. J. Chou, P. S. Ho, *J. Biol. Chem.* **1992**, 267, 11846-11855.

[11] A. Rich, S. Zhang, *Nat. Rev. Genet.* **2003**, 4, 566-572.

[12] G. Wang, K. M. Vasquez, *Mutat. Res.* **2006**, 598, 103-119.

[13] M. A. Fuertes, V. Cepeda, C. Alonso, J. M. Pérez, *Chem. Rev.* **2006**, 106, 2045-2064.

[14] Z. Wu, T. Tian, J. Yu, X. Weng, Y. Liu, Z. Zhou, *Angew. Chem. Int. Ed.* **2011**, 50, 11962-11967.

[15] L. J. Peck, A. Nordheim, A. Rich, J. C. Wang, *Proc. Natl. Acad. Sci. USA* **1982**, 79, 4560-4564.

[16] A. R. Rahmouni, R. D. Wells, *Science* **1989**, 246, 358-363.

[17] B. Wittig, S. Wölfl, T. Dorbic, W. Vahrson, A. Rich, *EMBO J.* **1992**, 11, 4653-4663.

[18] S. Rothenburg, F. Koch-Nolte, A. Rich, F. Haag, *Proc. Natl. Acad. Sci. USA* **2001**, 98, 8985-8990.

[19] D. -B. Oh, Y. -G. Kim, A. Rich, *Proc. Natl. Acad. Sci. USA* **2002**, 99, 16666-16671.

[20] R. Liu, H. Liu, X. Chen, M. Kirby, P. O. Brown, K. Zhao, *Cell* **2001**, 106, 309-318.

[21] A. Herbert, K. Lowenhaupt, J. Spitzner, A. Rich, *Proc. Natl. Acad. Sci. USA* **1995**, 92, 7550-7554.

[22] T. Schwartz, J. Behlke, K. Lowenhaupt, U. Heinemann, A. Rich, *Nat. Struct. Biol.* **2001**, 8, 761-765.

[23] S. Rothenburg, N. Deigendesch, K. Dittmar, F. Koch-Nolte, F. Haag, K. Lowenhaupt, A. Rich, *Proc. Natl. Acad. Sci. USA* **2005**, 102, 1602-1607.

[24] Y. -G. Kim, M. Muralinath, T. Brandt, M. Pearcy, K. Hauns, K. Lowenhaupt, B. L. Jacobs, A. Rich, *Proc. Natl. Acad. Sci. USA* **2003**, 100, 6974-6979.

[25] S. C. Ha, N. K. Lokanath, D. Van Quyen, C. A. Wu, K. Lowenhaupt, A. Rich, Y. -G. Kim, K. K. Kim, *Proc. Natl. Acad. Sci. USA* **2004**, 101, 14367-14372.

[26] A. Takaoka, Z. Wang, M. K. Choi, H. Yanai, H. Negishi, T. Ban, Y. Lu, M. Miyagishi, T. Kodama, K. Honda, Y. Ohba, T. Taniguchi, *Nature* **2007**, 448, 501-505.

[27] B. A. Brown II, K. Lowenhaupt, C. M. Wilbert, E. B. Hanlon, A. Rich, *Proc. Natl. Acad. Sci. USA* **2000**, 97, 13532–13586.

[28] S. C. Ha, K. Lowenhaupt, A. Rich, Y. -G. Kim, K. K. Kim, *Nature* **2005**, 437, 1183-1186.

[29] Y.-M. Kang, J. Bang, E.-H. Lee, H.-C. Ahn, Y.-J. Seo, K. K. Kim, Y.-G. Kim, B.-S. Choi, J.-H. Lee, *J. Am. Chem. Soc.* **2009**, 131, 11485-11491.

[30] S. Bae, D. Kim, K. K. Kim, Y. -G. Kim, S. Hohng, *J. Am. Chem. Soc.* **2011**, 133, 668-671.

[31] T. Ha, Th. Enderle, D. F. Ogletree, D. S. Chemla, P. R. Selvin, S. Weiss, *Proc. Natl. Acad. Sci. USA* **1996**, 93, 6264-6268.

[32] R. Roy, S. Hohng, T. Ha, *Nat. Methods* **2008**, 5, 507-516.

[33] X. Shi, J. Lim, T. Ha, *Anal. Chem.* **2010**, 82, 6132-6138.

[34] P. Hanggi, P. Talkner, M. Borkovec, *Rev. Mod. Phys.* **1990**, 62, 251-341.

[35] A. Herbert, J. Alfken, Y. -G. Kim, I. S. Mian, K. Nishikura, A. Rich A, *Proc. Natl. Acad. Sci. USA* **1997**, 93, 6264-6268.

[36] L. Zhang, S. Kasif, C. R. Cantor, N. E. Broude, *Proc. Natl. Acad. Sci. USA* **2004**, 101, 16855-16860.

[37] P. Khuu, M. Sandor, J. DeYoung, P. S. Ho, *Proc. Natl. Acad. Sci. USA* **2007**, 104, 16528-16533.

[38] H. Li, J. Xiao, J. Li, L. Lu, S. Feng, P. Dröge, *Nucl. Acids Res.* **2009**, 37, 2737-2746.

[39] R. Z. Cer, K. H. Bruce, U. S. Mudunuri, M. Yi, N. Volfovsky, B. T. Luke, A. Bacolla, J. R. Collins, R. M. Stephens, *Nucl. Acids Res.* **2011**, 39, D383-D391.

Abstract in Korean (국문초록)

단일분자 FRET을 이용한 Z-DNA에 대한 연구

서울대학교 물리천문학부

생물물리학 전공

배상수

지난 20세기 동안 생물학은 많은 발전을 이루어 왔다. 특히 1953년 왓슨과 크릭이 모든 생명체의 유전정보를 담고 있는 DNA의 구조를 밝혀냄으로써 <분자생물학>이라는 새로운 장이 열리게 되었다. 왓슨과 크릭이 제안한 DNA의 구조를 보면 (B-DNA라고도 불린다) 이중나선형태를 지녔는데 그 방향이 오른나선 방향이다. 이러한 구조는 이후 다양한 연구를 통해 검증이 되었다.

그런데 1979년 알렉산더 리치 그룹이 밝혀낸 DNA에 대한 최초의 크리스탈 구조를 보면 놀랍게도 오른나선이 아닌 왼나선의 DNA 이중구조였다 (이름을 Z-DNA라고 지었는데, 이는 백본의 형태가 지그재그여서 붙여졌다). Z-DNA의 구조를 보면 B-DNA와는 다른 점들이 많이 있다. Z-DNA는 이중나선의 방향이 왼나선이고, B-DNA에 비해 전체적으로 가늘고 긴 구조를 가지고 있다. Z-DNA는 보통의 생리학 조건에서는 거의 존재하지 않는데, 높은 농도의 이온이나 (-) supercoiling, DNA 염기의 조작, 그리고 특정 단백질이 있는 조건에서 쉽게 만들어 진다고 알려져 있다. Z-DNA가 발견된 이후 30 여년 동안 생물학적 역할에 대해 많은

연구가 이루어져 왔는데, 유전 조절과정에서 시작부분 그리고 뉴클레오솜의 위치변경 과정이나 유전자 불안정에 영향을 미치는 것으로 밝혀졌다.

Z-DNA에 대한 연구는 기존의 앙상블 실험에서는 한계가 있었다. 실제 Z-DNA는 많은 양의 B-DNA에 둘러 쌓여 있기 때문에 B-DNA의 신호로 인해서 Z-DNA에 대한 신호를 측정하는데 어려움이 있었다. 이를 극복하기 위해 우리는 단일분자 프렛을 이용한 단일분자에 대한 실험을 진행하였다. 우리는 단일분자 수준에서 높은 농도의 이온이나 단백질에 의한 B-Z 변이를 성공적으로 측정할 수 있었고 그 결과 다음과 같은 점들을 밝혀내었다.

1) 우리는 단일분자 프렛과 원평광 이색성을 이용하여 여러 가지 종류의 이온들에 대해서 Z-DNA 유도 능력을 측정하였다. 그 결과 기존에 높은 농도 조건에서 Z-DNA가 잘 생겨나는 이유로 널리 알려진 <정전기 가로막기> 효과와는 다르게, 호프마이스터 효과에 따라 Z-DNA가 잘 유도된다는 사실을 밝혀냈다.

2) 우리는 단일분자 프렛을 이용하여 본래적으로 존재하는 B-Z 변이과정과 단백질의 결합/분리 과정을 측정할 수 있었다. 이 결과 단백질에 의한 B-Z 변이는 능동적으로 유도 되는게 아니라, 단백질은 단지 수동적으로 본래적으로 생기는 Z-DNA에 잘 결합해서 Z-DNA를 안정화시킨다는 것을 밝혀냈다.

3) 우리는 DNA 뿐 아니라, RNA와 DNA, RNA가 결합한 하이브리드 형태의 샘플에 대해 단백질에 의한 Z-형태의 구조가 생겨나는 것을 관측하는데 성공하였다. 그 결과 DNA, RNA가

결합한 하이브리드 형태의 샘플이 다른 DNA와 RNA에 비해 더 빠르고 더 잘 Z-형태의 구조로 잘 변한다는 사실을 밝혀냈다. 이 결과로부터 모델을 세워, (시토신-구아닌) 반복 염기와 정션이 미치는 영향에 대해 각각 계산을 해내었다. 결과적으로 DNA, RNA가 결합한 하이브리드 형태의 샘플이 Z-형태의 구조로 가장 잘 변한다는 이유는 정션에서의 자유에너지 장벽이 제일 낮기 때문으로 드러났다.

핵심어: Z-DNA, BZ 변이, Z-DNA 유도 단백질, 단일분자 FRET, 호프마이스터 효과, DNA-RNA 결합

학번: 2008-30118